

**SEDS-Proceedings  
of the 8<sup>th</sup> GRS Workshop**

**Safety of Extended  
Dry Storage of Spent  
Nuclear Fuel**

**Garching,  
15<sup>th</sup> – 17<sup>th</sup> May 2024**

**SEDS-Proceedings  
of the 8<sup>th</sup> GRS Workshop**

**Safety of Extended  
Dry Storage of Spent  
Nuclear Fuel**

**Garching,  
15<sup>th</sup> – 17<sup>th</sup> May 2024**

Florian Rowold  
Oliver Bartos  
Klemens Hummelsheim

September 2024

**Remark:**

This report refers to research project 4721E03330 which has been funded by the German Federal Ministry for the Environment, Nature Conservation, Nuclear Safety and Consumer Protection (BMUV).

The work was conducted by GRS.

The responsibility for the content of the report lies with the authors.

All data and information contained in the SEDS 2024 proceedings are subject to copyright and intellectual property rights.

The authors and their affiliated institutions hold the rights to their respective contributions.

Any use, reproduction, distribution, or modification of the data presented in these proceedings requires express authorisation from the authors and their affiliated institutions.

Furthermore, any commercial or non-commercial use of the data must be approved by the authors.

For inquiries regarding data usage or requests for authorisation, please contact the contributing authors.

**Keywords**

Ageing Management, Cladding, Dry Storage, Inventory, Safety of the extended dry Storage of spent nuclear Fuel, Spent Fuel, SEDS 2024

## Introduction

All countries with nuclear power plants do not currently have a repository for high-level radioactive waste in operation. This means that in most countries there is a need to store radioactive waste, such as spent fuel, for longer than planned.

The Safety of Extended Dry Storage of Spent Nuclear Fuel (SEDS) workshop was launched in 2017 as a small, focused conference on progress in the safety aspects of extended dry storage of spent nuclear fuel. The aim is to identify knowledge gaps for extended storage and to exchange ideas with research and expert organisations mainly from Germany, the EU and Switzerland. In 2019, the SEDS workshop gained international recognition as an affiliate of the EPRI-ESCP meeting. Since then, the workshop has become an important event in the international field of extended storage. During the COVID-19 pandemic, the workshop was also held in digital form in 2020 and 2021 with about 100 participants. From a scientific point of view, numerous research topics emerged from the exchange at the SEDS workshop, which also led to new collaborations. It was possible to identify existing knowledge gaps for safe extended storage and to define corresponding research areas.

The Gesellschaft für Anlagen- und Reaktorsicherheit (GRS) gGmbH hosts its 8<sup>th</sup> SEDS workshop in Garching near Munich on 15<sup>th</sup> – 17<sup>th</sup> May 2024. The event attracted great attention as the program was filled with 18 presentations from 16 institutes and attended by 49 experts from 8 countries. For Germany, the broad range of experts was represented by universities and research organizations, technical support organizations, fuel suppliers and authorities.



## Content

	<b>Introduction.....</b>	<b>I</b>
	<b>Content.....</b>	<b>III</b>
<b>1</b>	<b>Agenda .....</b>	<b>1</b>
<b>2</b>	<b>Titles of the Lectures of the Authors.....</b>	<b>3</b>
2.1	IAEA Activities related to Extended Storage of Fuel.....	5
2.2	BGZ's Research Programme - Update and Overview .....	6
2.3	Feasibility of passive measurements of the peak temperature of the cladding in a spent fuel cask during fuel transfer.....	7
2.4	Self-limitation of cladding creep in dry storage.....	11
2.5	Extended Storage of Spent Nuclear Fuel in Casks, Inventory Assessment using Fuel Rod Performance Codes - An Update and recent Developments .....	16
2.6	Spent Fuel Safety Analysis during Dry Storage through Fuel (GIFT) and Thermal analysis (COBRA-SFS) Integrated Code .....	23
2.7	Structural Response of Reinforced Concrete Structures under Impact Loading.....	24
2.8	Evaluation of load scenarios for Spent Fuel Assemblies .....	30
2.9	Impact of Modeling Assumptions on Muon Scattering Images of Loaded Dry Storage Casks,.....	33
2.10	Radiation-based methods for non-invasive monitoring of transport and storage casks .....	36
2.11	Update of the SPIZWURZ project.....	37
2.12	SPIZWURZ Benchmark for simulation of hydrogen behaviour in fuel rod claddings at dry storage relevant conditions. Phase 1 (Blind tests)....	39
2.13	Evaluation methodology of spent fuel mechanical performance under UO <sub>2</sub> oxidation in dry management .....	41
2.14	Investigation of chemical and mechanical properties of irradiated Zircaloy possibly influencing the structural integrity during dry (long-term) interim storage.....	49
2.15	Activities of Axpo in the field of fuel integrity during dry storage .....	51

2.16	Activities related to the characterization of spent nuclear fuels by Tractebel .....	53
2.17	Investigating the Applicability of the Master Curve Concept for Ductile Cast Iron – Early Results for 2 Different Test Temperatures, .....	59
2.18	An update on metal seal tests performed at BAM and implications for interim storage,.....	65

# 1 Agenda

## 8<sup>th</sup> GRS Workshop on the Safety of Extended Dry Storage of Spent Nuclear Fuel

15-17<sup>th</sup> May 2024 hosted by Gesellschaft für Anlagen- und Reaktorsicherheit (GRS)  
gGmbH

Wednesday, 15<sup>th</sup> May 2024

Time	Title	Speaker/ Organization
12:00	Snacks & Drinks	
13:00	Welcoming and Workshop Overview	Chairs
13:20	IAEA Activities related to Extended Storage of Fuel	C. Gastl, IAEA
13:50	BGZ's Research Programme - Update and Overview	M. Stuke, BGZ
14:20	Coffee break	
14:40	Feasibility of passive measurements of the peak temperature of the cladding in a spent fuel cask during fuel transfer	S. Caruso, KKG
15:10	Self-limitation of cladding creep in dry storage	R. Sedlacek, Framatome
15:40	Coffee Break	
16:00	Extended Storage of Spent Nuclear Fuel in Casks, Inventory Assessment using Fuel Rod Performance Codes An Update and recent Developments	G. Spykman, TÜV Nord
16:30	Spent Fuel Safety Analysis during Dry Storage through Fuel (GIFT) and Thermal analysis (COBRA-SFS) Integrated Code	C. Lee, SNU
17:00	Coffee Break & End of Session	
18:00	Buffet @ GRS in Garching	

Thursday, 16<sup>th</sup> May 2024

Time	Title	Speaker/ Organization
09:00	Coffee & Tea	
09:30	Structural Response of Reinforced Concrete Structures under Impact Loading	L. Heibges, RPTU
10:00	Evaluation of load scenarios for Spent Fuel Assemblies	K. Simbruner, GRS
10:30	Coffee Break	
11:00	Impact of Modeling Assumptions on Muon Scattering Images of Loaded Dry Storage Casks	J. Niedermeier, TUM

11:30	Radiation-based methods for non-invasive monitoring of transport and storage casks	S. Eisenhofer, TUD
12:00	Lunch Break	
13:15	Update of the SPIZWURZ project	S. Weick, KIT
13:45	SPIZWURZ Benchmark for simulation of hydrogen behaviour in fuel rod claddings at dry storage relevant conditions. Phase 1 (Blind tests)	A. Rezhikova, GRS
14:15	Coffee Break	
14:45	Evaluation methodology of spent fuel mechanical performance under UO <sub>2</sub> oxidation in dry management	C. Aguado, CIEMAT
15:15	Investigation of chemical and mechanical properties of irradiated Zircaloy possibly influencing the structural integrity during dry (long-term) interim storage	T. Lin, KIT
15:45	End of Session	
19:00	Dinner @ Hofbräukeller in München	

Friday, 17<sup>th</sup> May 2024

Time	Title	Speaker/ Organization
09:00	Snacks & Drinks	
09:30	Activities of Axpo in the field of fuel integrity during dry storage	M. Zemek, Axpo
10:00	Works related to the characterization of spent nuclear fuel by Tractebel	A. Dethioux, Tractebel
10:30	Coffee Break	
10:50	Investigating the Applicability of the Master Curve Concept for Ductile Cast Iron – Early Results for 2 Different Test Temperatures	M. Holzwarth, MPA
11:20	An update on metal seal tests performed at BAM and implications for interim storage	M. Jaunich, BAM
11:50	Summary and Discussion of the Workshop	All
12:10	End of Workshop	

## 2 Titles of the Lectures of the Authors

1. IAEA Activities related to Extended Storage of Fuel, Cristoph Gastl, International Atomic Energy Agency (IAEA), Austria
2. BGZ's Research Programme - Update and Overview, Maik Stuke, Gesellschaft für Zwischenlagerung (BGZ), Germany
3. Feasibility of passive measurements of the peak temperature of the cladding in a spent fuel cask during fuel transfer, Stefano Caruso, Kernkraftwerk Gösgen-Däniken AG (KKG), Switzerland
4. Self-limitation of cladding creep in dry storage, Radan Sedlacek, Framatome GmbH, Germany
5. Extended Storage of Spent Nuclear Fuel in Casks, Inventory Assessment using Fuel Rod Performance Codes - An Update and recent Developments, Gerold Spykman, TÜV Nord, Germany
6. Spent Fuel Safety Analysis during Dry Storage through Fuel (GIFT) and Thermal analysis (COBRA-SFS) Integrated Code, Chansoo Lee, Seoul National University (SNU), Southkorea
7. Structural Response of Reinforced Concrete Structures under Impact Loading, Lars Heibges, Rheinland-Pfälzische Technische Universität (RPTU), Germany
8. Evaluation of load scenarios for Spent Fuel Assemblies, Kai Simburner, Gesellschaft für Anlagen – und Reaktorsicherheit (GRS) gGmbH, Germany
9. Impact of Modeling Assumptions on Muon Scattering Images of Loaded Dry Storage Casks, Julia Niedermeier, Technische Universität München (TUM), Germany
10. Radiation-based methods for non-invasive monitoring of transport and storage casks, Suzanne Eisenhofer, Technische Universität Dresden (TUD), Germany
11. Update of the SPIZWURZ project, Sarah Weick, Karlsruhe Institut for Technology (KIT), Germany
12. SPIZWURZ Blind Benchmark for simulation of hydrogen behaviour in fuel rod claddings at dry storage relevant conditions. Aleksandra Rezchikova, Gesellschaft für Anlagen – und Reaktorsicherheit (GRS) gGmbH, Germany
13. Evaluation methodology of spent fuel mechanical performance under UO<sub>2</sub> oxidation in dry management, Carlos Aguado, CIEMAT, Spain
14. Investigation of chemical and mechanical properties of irradiated Zircaloy possibly influencing the structural integrity during dry (long-term) interim storage, Yvonne Lin, Karlsruhe Institut for Technology (KIT), Germany

15. Activities of Axpo in the field of fuel integrity during dry storage, Martin Zemek, Axpo Power AG, Switzerland
16. Works related to the characterization of spent nuclear fuel by Tractebel, Adrien Dethioux, Tractebel, Belgium
17. Investigating the Applicability of the Master Curve Concept for Ductile Cast Iron – Early Results for 2 Different Test Temperatures, Marcel Holzwarth, Materials Testing Institute University of Stuttgart (MPA), Germany
18. An update on metal seal tests performed at BAM and implications for interim storage, Matthias Jaunich, Bundesamt für Materialforschung (BAM), Germany

**2.1 IAEA Activities related to Extended Storage of Fuel**

*Christoph Gastl*

*International Atomic Energy Agency (IAEA), Austria*

N/A

## **2.2 BGZ's Research Programme - Update and Overview**

*Maik Stuke*

*Gesellschaft für Zwischenlagerung mbH (BGZ), Germany*

N/A

## 2.3 Feasibility of passive measurements of the peak temperature of the cladding in a spent fuel cask during fuel transfer

*Stefano Caruso<sup>1</sup>, Achim Hofmann<sup>1</sup>, Alexandra Alander<sup>1</sup>,  
Marie Benoit<sup>2</sup>, Stephane Nallet<sup>2</sup>*

<sup>1</sup> *Kernkraftwerk Gösgen-Däniken AG (KKG), Switzerland*

<sup>2</sup> *ORANO NPS – R&D, France*

### **Abstract**

A new measurement technique utilizing irreversible temperature-indicating lacquers has been developed and tested, demonstrating its effectiveness in indicating temperature peaks in spent nuclear fuel cladding without requiring active monitoring systems during routine transfers of spent fuel at Gösgen Nuclear Power Plant (KKG). Another novel and different measurement technique based on a purely mechanical principle, was developed by Orano NPS and also tested at KKG. The preliminary results are in agreement, although they remain at a qualitative level. Specific calculations are planned for further comparison between predicted and measured values.

### **Introduction**

The cladding temperature is crucial for assessing of spent fuel performance during dry storage. Existing measurement techniques are often impractical for regular use under operational conditions, necessitating the development of new methods, which were realized and tested in three major campaigns in 2011, 2022 and 2023 at the Gösgen Nuclear Power Plant.

### **Implementing Irreversible Temperature-Indicating Lacquers**

The measurement of temperature using the irreversible temperature-indicating lacquers [1] is based on a procedure in which a lacquer is applied to a surface and then subjected to a process that permanently alters its physical properties. The pigment undergoes a color change upon reaching its melting point, which indicates the surpassing of certain temperature thresholds. By utilizing different substances with varying melting points across multiple areas, a multitude of temperature ranges can be addressed. A total of 13 temperature levels were covered by the different lacquers used at the KKG, with temperatures ranging from 149 °C to 454 °C. Some cylindrical supports with notches were manufactured and the lacquers supports were machined on aluminum bars to avoid radioactive activation. Lacquer was applied to each notch of the bar (see Fig.1). Subsequently, the sensors were encapsulated (welded) in steel tubes and each inserted into the guide

tubes of the fuel assembly (FA). This operation was performed under water in the internal wet storage pool of KKG [2]. The encapsulation is required to ensure the sensor remains completely dry, preventing contact between the pigments and the water in the pool and avoiding the damage to the lacquers. The FA hosting the sensor was loaded into the transport cask, in the central position. The cask belongs to the series TN12, which is used as a shuttle in KKG to transfer the FAs within the power plant area. The cask is capable of accommodating 12 FAs. Following the closure of the cask, the content of the cask was subjected to vacuum drying and placed under a helium atmosphere. The cask was subsequently transferred from the internal wet storage pool to the external wet storage pool of KKG. Once the cask was opened and the FAs unloaded and stored in their box position in the pool, the probes were withdrawn from the assemblies and the steel tubes opened in the KKG hot workshop.

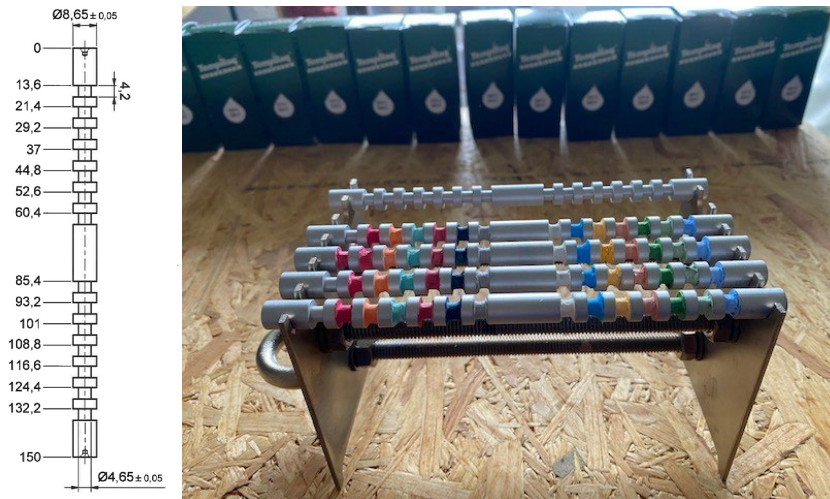


**Fig. 1** Lacquers temperature indicators: design of the supports for the aluminium support (left) and final sensors (right) [2]

### Implementing Bimetallic Washers Temperature-Indicators

Orano NPS is developing a passive temperature sensor to measure the maximal temperature of the spent fuel cladding inside a transport cask during transport. The sensor is designed to be inserted into the guide tubes of spent fuel assemblies, as for the case of lacquers illustrated above. The sensor is an assembly of bimetallic washers disposed along a central rod and inserted within a stainless-steel tube measuring 300 mm in length (see Fig. 2). A plug is welded at both the bottom and the top of the tube. A system comprising an internal movable trolley and teeth machined on the external stainless tube is employed to measure the maximal temperature reached. The trolley is designed to move up in response to thermal expansion of the washers and is unable to return to its original

position when the temperature decreases. The new position reached by the trolley following the completion of transport operations and its unloading will allow to determine the maximal cladding temperature. This can be possible in combination with the calibration of the sensor performed by Orano, prior to the sensor's delivery to KKG. The sensor exhibits a linear response to an increase in temperature, with an estimated uncertainty of 10 °C. The encapsulation procedure in welded steel tubes is analogous to that of lacquers, as previously described. This was performed by KKG. The insertion of the sensors into the guide tubes of the FA was conducted by the Framatome fuel service team. The retrieval operations are also identical to those previously conducted for the lacquers.



**Fig. 2** ORANO temperature sensors composed of bimetallic washers inside a stainless-steel tube.

### **Experimental campaigns and first evaluation**

The 2022 campaign utilized several lacquers, each covering a different temperature range, to measure peak cladding temperatures during the transfer of SNF between the internal and external spent fuel pools. The sensors were placed inside the fuel assembly guide tubes, and temperature readings were obtained post-transfer, demonstrating the practicality and effectiveness of the technique in operational environments. Evaluations from the 2022 campaign indicated successful temperature measurement with lacquers, although the technique primarily offers qualitative results. The data collected are in fact indicative, showing that certain temperature thresholds were not exceeded, thereby validating the safety parameters set for SNF dry storage.

During the 2023 transfer campaign two prototypes of the ORANO temperature sensors have been tested during an internal transfer of twelve fuel assemblies. Another lacquers-based temperature indicator was loaded in the same FA. The results from the two types

of technologies are found to be in good agreement, showing a temperature below 300°C. Further calculations of fuel cladding temperatures will be performed by Orano NPS for comparison with experimental values.

### **Conclusions**

The study confirms the efficacy of using passive techniques for monitoring peak cladding temperatures in SNF transport casks. Despite some limitations in resolution and quantitative assessment, the methods provide a practical tool for ensuring compliance with safety standards during the transport and storage of SNF. The results obtained will be compared with simulations. Furthermore, the development of the ORANO sensors is currently progressing, aiming to further optimize the technology. Further campaigns at KKG are being considered.

### **Acknowledgments**

The authors would like to acknowledge the numerous team members at KKG who provided invaluable technical assistance during the implementation of the sensors. Additionally, the authors would like to express their appreciation to the Framatome Fuel service team for their expertise in handling and extracting the sensors.

### **References**

- [1] Tempilaq pigments from ISO OERLIKON AG.
- [2] S. Caruso, et al., Measurements of peak cladding temperature in spent fuel cask during fuel transfer, Proceedings of the 20th International Symposium on the Packaging and Transportation of Radioactive Materials (PATRAM 22), 1-15 June 2023, Juan-les-Pins, France.

## 2.4 Self-limitation of cladding creep in dry storage

*Radan Sedláček, Dietmar Deuble*

*Framatome GmbH, Germany*

The effect of self-limitation of cladding creep in dry storage was mentioned by U.S. NRC [1]. It is claimed that the cladding hoop stress decreases because the fuel rod free volume increases by cladding creep. This reduces the gas pressure within the fuel column with a corresponding decrease in cladding hoop stresses. The net effect is a slow decrease in pressure and hoop stress with increasing creep strain [1]. This effect should not be confused with the hoop stress decrease due to decreasing temperature in dry storage. The above statement seems to be in contradiction to the known fact that in gas-tight welded, pre-pressurized hollow cladding creep samples with constant amount of gas, Figure 1 the hoop stress remains constant during creep.



**Fig. 1** Gas-tight welded, pre-pressurized hollow cladding creep sample used in [4].

To analyse the effect of self-limitation of cladding creep, we separate the temperature and creep strain dependence of gas pressure [5]. Initial hoop stress in the undeformed cladding,  $\sigma_{\theta,ini}$  can be estimated as

$$\sigma_{\theta,ini} = p_{i,ini} \frac{r_{ini}}{w_{ini}} \quad (1)$$

where  $p_{i,ini}$  is the internal gas pressure,  $r_{ini}$  the cladding radius,  $w_{ini}$  the cladding wall thickness. The cladding deformation is represented by tangential creep strain  $\epsilon_{\theta}$ , radial creep strain  $\epsilon_r$  and axial creep strain  $\epsilon_z$ . When considering logarithmic strains, the deformed cladding radius  $r$ , deformed wall thickness  $w$  and deformed length  $l$  are

$$r = r_{ini} \exp(\epsilon_{\theta}) \quad w = w_{ini} \exp(\epsilon_r) \quad l = l_{ini} \exp(\epsilon_z) \quad (2)$$

Elastic strains are neglected. The creep deformation is material volume conserving,

$$\varepsilon_{\theta} + \varepsilon_r + \varepsilon_z = 0 \quad (3)$$

Relations between the individual strain components  $\varepsilon_{\theta}$ ,  $\varepsilon_r$ ,  $\varepsilon_z$  depend on cladding anisotropy.

Volume of a hollow cylinder is proportional to its length times radius square,  $V_H = \pi r^2 l$  so internal volume of the deformed cladding is

$$V_H = V_{H,ini}(\exp(\varepsilon_{\theta}))^2 \exp(\varepsilon_z)$$

If a fraction  $0 \leq k < 1$  of the initial cladding volume  $V_{H,ini}$  is occupied by pellets with volume  $V_P = kV_{H,ini}$ , see Figure 2, the free volume of the undeformed cladding is

$$V_{F,ini} = V_{H,ini} - V_P = V_{H,ini}(1 - k) \quad (4)$$

The free volume of the deformed cladding then becomes

$$V_F = V_{H,ini}((\exp(\varepsilon_{\theta}))^2 \exp(\varepsilon_z) - k)$$

A negative value of the filling fraction  $k < 0$  is also admissible. It has the meaning of an additional plenum that increases the free volume beyond that of the cylindrical sample itself and the walls of which do not creep, Fig. 2.

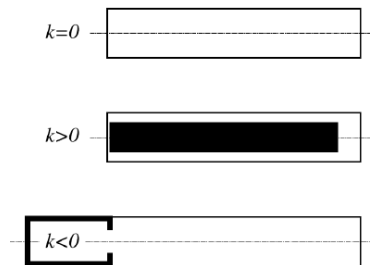


**Fig. 2** Pre-pressurized hollow sample ( $k = 0$ ), sample (fuel rod) filled with pellets ( $k > 0$ ), and pre-pressurized sample with additional non-creeping plenum ( $k < 0$ ) [5].

According to Boyle-Mariotte law, internal pressure at constant gas amount and constant temperature is inversely proportional to free volume,  $p_i \cdot V_F = \text{const}$ , so the internal pressure in the deformed cladding changes as

$$\frac{p_i}{p_{i,ini}} = \frac{V_{F,ini}}{V_F} = \frac{1 - k}{(\exp(\varepsilon_\theta))^2 \exp(\varepsilon_z) - k} \quad (5)$$

Equation (5) represents the indirect effect of cladding creep on the cladding stress, namely the internal pressure decrease. Finally, the hoop stress in the deformed cladding can be expressed as

$$\frac{\sigma_\theta}{\sigma_{\theta,ini}} = \frac{p_i}{p_{i,ini}} \frac{r}{r_{ini}} \frac{w_{ini}}{w} = \frac{1 - k}{(\exp(\varepsilon_\theta))^2 \exp(\varepsilon_z) - k} \cdot \frac{\exp(\varepsilon_\theta)}{\exp(\varepsilon_r)} = \frac{1 - k}{1 - k \exp(\varepsilon_r - \varepsilon_\theta)} \quad (6)$$

where the direct effect of changing cladding dimensions on stress has been accounted for and the material volume conservation, eq. (3), was utilized.

In case of pre-pressurized hollow cladding ( $k = 0$ ), the decreasing internal pressure is compensated by changing cladding dimensions, the self-compensation is complete, the stress remains constant. In fuel rod filled with pellets ( $k > 0$ ), the internal pressure decreases more rapidly, the self-compensation by changing cladding dimensions is incomplete, the stress decreases as well. The amount of stress decrease is controlled by the filling fraction  $k$ . This is what is called self-limitation of cladding creep in dry storage: the creep rate decreases with creep strain [1]. Development of internal pressure, eq. (5), and hoop stress, eq. (6), with increasing tangential creep strain is shown in Fig. 3.

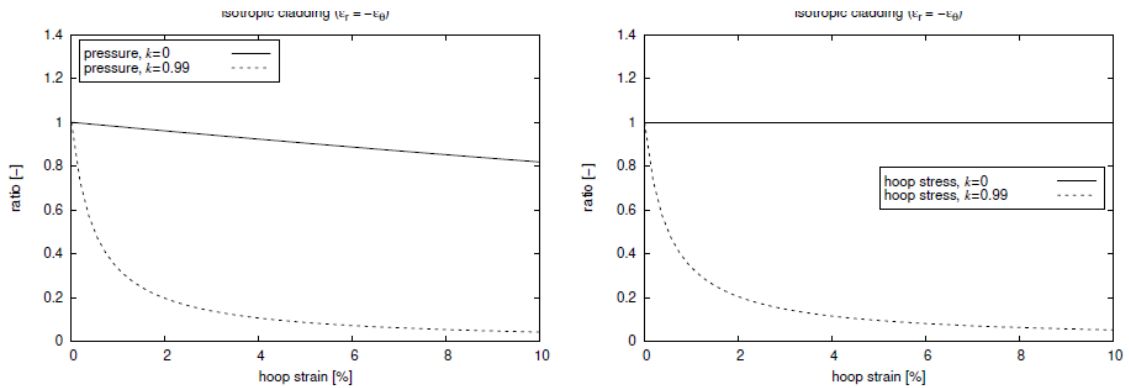


**Fig. 3** Internal pressure, eq. (5) (left) and hoop stress, eq. (6) (right) as functions of hoop strain for pre-pressurized hollow cladding ( $k = 0$ ) and pre-pressurized filled cladding ( $k > 0$ ).

The phenomenon of creep self-limitation in dry storage was assessed quantitatively in Ref. [5], using the above model and a fuel rod from the GRS benchmark [6] as an example. Due to the typical 2 temperature profile in the cask, Fig. 4, only about 1/3 of the active length, where the temperature is high enough, can creep significantly. A fuel

rod in dry storage is therefore, in terms of the present model, more like a filled sample represented by about one third of the active length, complemented by additional non-creeping volumes (lower plenum with the adjacent 1/3 of active length and upper plenum with the adjacent 1/3 of active length), Fig. 4. Using eq. (6), the net decrease in hoop stress due to increasing volume was estimated in [5] as

$$\frac{\sigma_{\theta}}{\sigma_{\theta,ini}} \approx 0.99997$$

This estimate has been confirmed by calculations using the Framatome dry storage code CSAS R&D [7], where the effect of creep self-limitation was switched on and off [5]. Compared to the stress decrease due to sinking temperature in dry storage, i.e. from initial 41.42MPa to final 29.18MPa, the discussed effect of creep self-limitation is negligible.

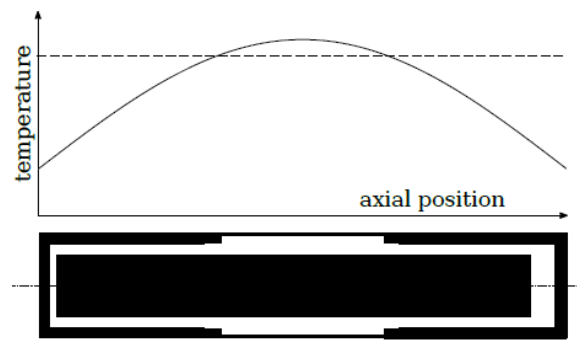


**Fig. 4** Schematic diagram of a fuel rod in dry storage with the corresponding axial temperature profile. The bold lines symbolize parts of the cladding where creep can be considered negligible in a first approximation. In terms of the model, those parts present additional non-creeping plena. The middle part corresponds to a creep sample with free volume in the gap between pellets and cladding.

Additionally, an upper bound estimate of possible contribution of the self-limitation effect to stress decrease in dry storage was performed, based on the assumption that maximum allowed tangential creep strain is 1%. The estimated maximum contribution of the creep self-limitation is then about 4% decrease in the hoop stress relative to its initial value [5].

## References

- [1] Dry Storage and Transportation of High Burnup Spent Nuclear Fuel. NUREG-2224, Final report, U.S.NRC, 2020.
- [2] M. Mayuzumi and T. Onchi. Creep deformation of an unirradiated Zircaloy nuclear fuel cladding tube under dry storage conditions. *Journal of Nuclear Materials*, 171:381{388, 1990.
- [3] C. Cappelaere, R. Limon, C. Duguay, G. Pinte, M. Le Breton, P. Bou\_oux, V. Chabretou, and A. Miquet. Thermal creep model for CWSR Zircaloy-4 cladding taking into account the annealing of the irradiation hardening. *Nuclear Technology*, 177(2):257{272, 2012.
- [4] R. Sedlacek and D. Deuble. Kinematic hardening in creep of Zircaloy. *Journal of Nuclear Materials*, 479:338{346, 2016.
- [5] R. Sedlacek and D. Deuble. Self-compensation in creep of pressurized cladding tubes: From self-limitation in dry storage to self-acceleration in burst tests. *Nuclear Engineering and Design*, 413:112480, 2023.
- [6] F. Boldt, M. Stuke, and M. P\_eridis. Benchmark on Thermomechanical Fuel Rod Behaviour, Phase I Report. GRS-671, Gesellschaft für Anlagen- und Reaktorsicherheit (GRS) gGmbH, 2022.
- [7] R. Sedl\_a\_cek, D. Deuble, H. Landskron, and E. Schweitzer. Benchmark for thermo-mechanical fuel rod behaviour during dry storage. In F. Boldt, M. Stuke, and M. Peridis, editors, *Benchmark on Thermomechanical Fuel Rod Behaviour, Phase I Report*, pages 101-103. Gesellschaft für Anlagen- und Reaktorsicherheit (GRS) gGmbH, 2022.

## **2.5 Extended Storage of Spent Nuclear Fuel in Casks, Inventory Assessment using Fuel Rod Performance Codes - An Update and recent Developments**

*Gerold Spykman*

*TÜV Nord EnSys GmbH & Co.KG, Germany*

In the paper on extended storage of spent nuclear fuel [4], which was presented at the previous SEDS meeting, we explored the current assessment methods for fuel performance during dry storage and possible future approaches. Within this paper we present the updated status of this work and respond to some recent developments. The aim of the project is to establish methods and a prototype tool to assess the fuel performance in dry cask for a prolonged storage time up to 100 years and longer. As before, we use the TRANSURANUS fuel performance code [1], [2] with an adapted input generation desk. The necessary fuel data is provided by our TITANIA [3] database.

In March 2023, ESK published a position paper on the “Extended storage of spent nuclear fuel and other high-level radioactive Waste depending on the selection of the repository site” [5], in which they addressed the temporal aspects of extended interim storage and the verification procedures for the necessary permits. The ESK considers an interim storage period of 120 years with possible extensions. Further points include knowledge retention and data availability as well as a set of rules detailing that the safety-related verification should be based on a protection-goal-oriented approach. In particular, the handling of uncertainties and conservatism must be regulated. Here, we pursue a very similar goal, which was our original intention for this project.

Throughout the work on the prototype, we have gained some new insights: First, we found, that the orientation (rotation) of the fuel assembly in the cask compartment is neither specified nor documented. So, the orientation has to be implemented as another statistical parameter in the probabilistic assessment. Within the existing verification procedure some parameter like post irradiation decay power, burn up and the calculation of temperatures are determined in a conservative manner that cannot be used in a probabilistic approach as varied parameters. If best estimate and uncertainties are not available these parameters have to be evaluated as fixed parameters, which poses another challenge.

What are the new implementations in the software prototype since the last SEDS meeting in 2023? One main novelty is the refinement of the time step control within the timeline creation process and the calculation of the temperatures within the cask from the decay heat of the fuel assemblies. Figures 1 and 2 depict the computed temperatures and decay power for a 33-kW loading of a CASTOR V/19 cask at loading time. The maximum temperature is about 302 °C in the center of the cask. The maximum average fuel rod decay power is less than 0.026 W/cm. In addition to the afore mentioned capabilities, we also implemented new visualization options and improved the timeline analyzing desk (figure 3). The latter is very helpful for checking input data and for documentation of the QC-processes.

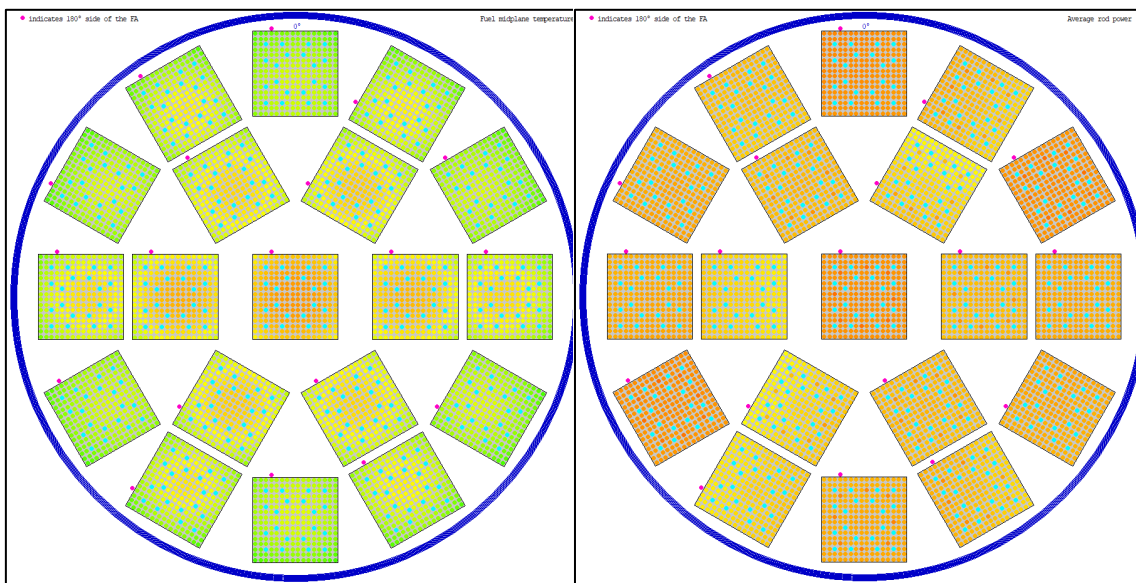


**Fig. 1** Temperature distribution within the cask at loading time (scale: 20 °C to 370 ° C)  
 (© TÜV NORD EnSys GmbH Co.KG)

**Fig. 2** Fuel rod average decay power at loading time (scale: 0 W/cm to 0.026 W/cm)  
 (© TÜV NORD EnSys GmbH Co.KG)

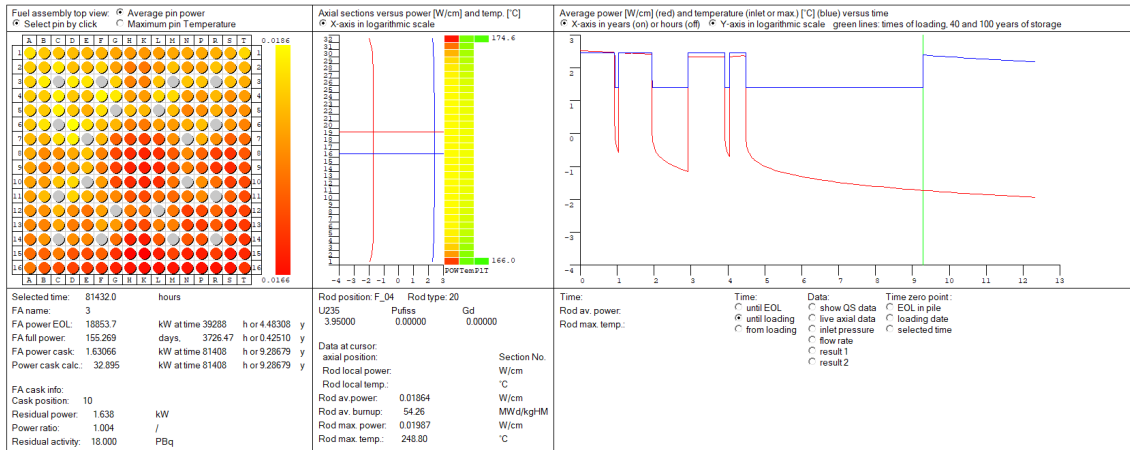


**Fig. 3** Timeline analyzing deck (© TÜV NORD EnSys GmbH Co.KG)

An automated documentation of the chosen models, varied parameter and diced values for each run has been implemented as well in order to trace back the results to its input parameters. In the next step we also improved the output schemes. Since the data that should be included in the output scheme depends on the specific tasks, the improvement of the output scheme is an ongoing challenge within this work. An example of an output scheme and visualization deck is shown in figure 4.

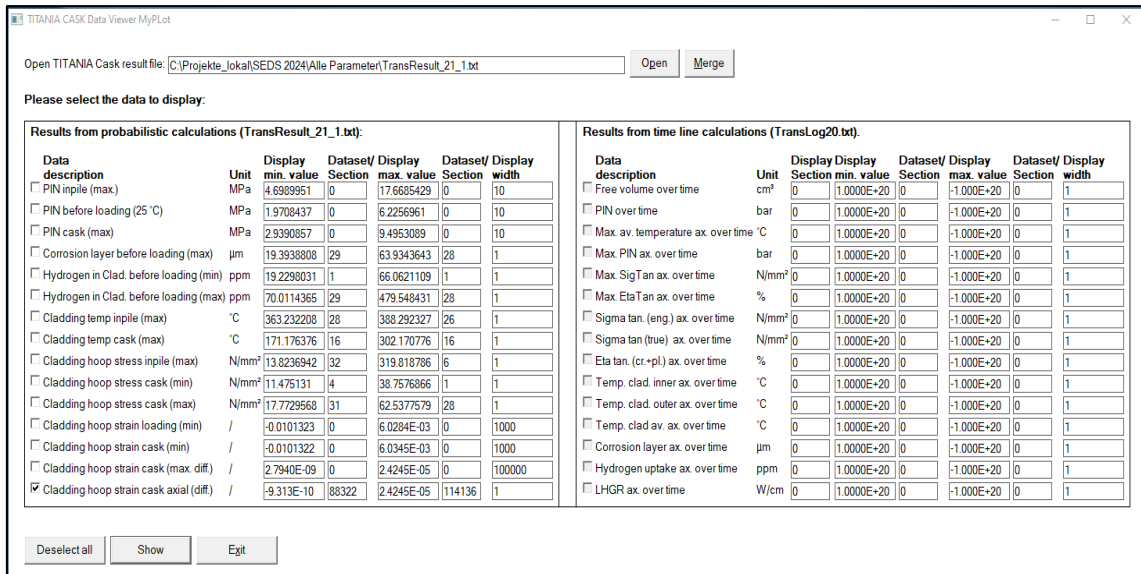


**Fig. 4** Example of an output scheme and visualization deck (© TÜV NORD EnSys GmbH Co.KG)

Since the SEDS 2023, we performed many calculations for testing the stability of the prototype software, validating the model, and improving on the input-and output desks.

Within this paper and presentation, we will focus on some specific results of three cases of full cask calculations. In all three cases we consider the loading of CASTOR V/19 cask with 19 PWR fuel assemblies with a 16x16 fuel rod layout and 20 guiding tubes per assembly. This amounts to a total of 4484 fuel rods, whose parameters can be varied. In the first case, we performed best estimate calculations without any parameter variations. This results in 4484 calculations. In the second case, we varied the inner and outer radius of the cladding only. This case consists of 100.000 calculations and had an error count of zero. The error count indicates cases where the fuel rod performance code end with an error code greater than zero. This can be caused by non-physical parameter combinations. The third case also comprises 100.000 single calculations with variations of all fuel rod parameter (inner parameter). The error count within this case was less than 200. The in-pile, wet pool, and dry storage boundary conditions parameter (outer parameter) are the same as in the best estimate calculation case.

These calculations produce a huge amount of data for the analysis of the impact of many different parameters. In the following, we focus on the following parameters: initial (cold) rod pressure before loading, maximum hoop stress during dry storage, and the maximum hoop strain increase during dry storage. These three parameters are important for the fuel rod assessment in today's method for the exclusion of a systematic fuel rod cladding failure during the 40-year licensed dry storage period in Germany.

Figure 5 depict the calculated maximum increase of the cladding hoop strain for the axial sections of a fuel rod during the dry storage (100 years) for the three calculation cases. As expected, the best estimate calculation (case 1) shows the smallest increase. The variation of the cladding radii (case 2) has an important impact on the cladding hoop strain, while the variation of all fuel rod parameter (inner parameter) in case 3 produces the greatest value for the hoop strain increase. Furthermore, the results show that the hoop strain increase follows the axial temperature distribution and the temperature over time. The creep properties are strongly temperature depending as well. We chose the parameter hoop strain increase during dry storage since in today's methodology the specified fuel rod manufacturing diameter including tolerances and cladding diameter reduction due to corrosion is used. This is a conservative approach regarding the maximum hoop stress in the cladding and therefore a maximum hoop strain increase of the cladding. Hence, this approach cannot be used for an integral calculation of the fuel rod life from the beginning of the first reactor cycle to the end of a long dry storage period. Since most of the fuel rods cladding are crept down to the outer fuel pellet radius, the

outer cladding radius at the beginning of dry storage is less than the entire manufacturing radius. Due to the in-pile radiation the stress component of creep has relaxed. Therefore, the initial state of the cladding of each individual fuel rod is the cold state before loading into the cask as calculated within this approach. The fuel rod performance during dry storage regarding cladding hoop strain is described by the hoop strain increase during dry storage time.

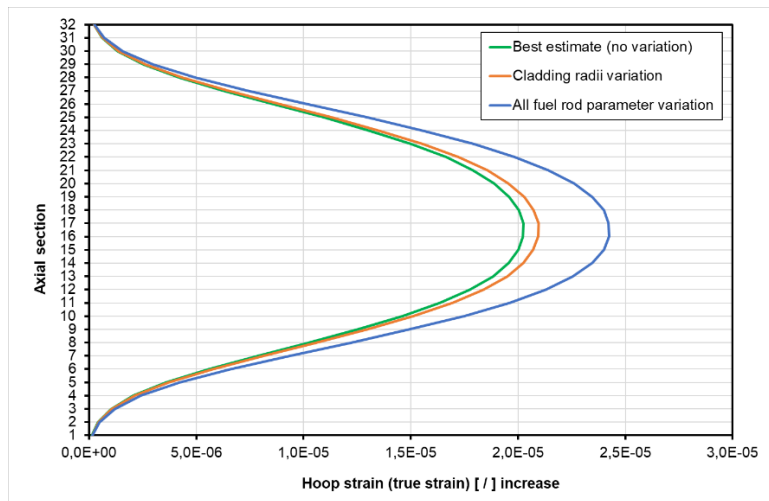


**Fig. 5** Cladding hoop strain increase for three calculation cases during 100 years of dry storage (© TÜV NORD EnSys GmbH Co.KG)

The following figure 6 shows the results for the inner pin pressure before loading, the maximum hoop stress and the hoop strain increase of the three calculation sets described above as distributions of the single calculation results. One must consider that the calculation case 1 is a best estimate calculation where every fuel rod is calculated once (4484 calculations). In the calculation cases 2 and case 3 there are 100.000 calculations shown from probabilistic determined rods of the population of 4484 rods within the cask loading. The ordinates of case 1 figures are scaled to 10 % of the ordinates of the case 2 and case 3 figures.

Within the distributions one can see that the hoop stress clearly follows the rod inner pressure. The rod inner pressure is the main parameter in the hoop stress variation since the variation of other parameter like the cladding diameters show here a minor effect on the result. The hoop stress increase distribution during dry storage show that most of all rods have a negligible hoop strain increase.

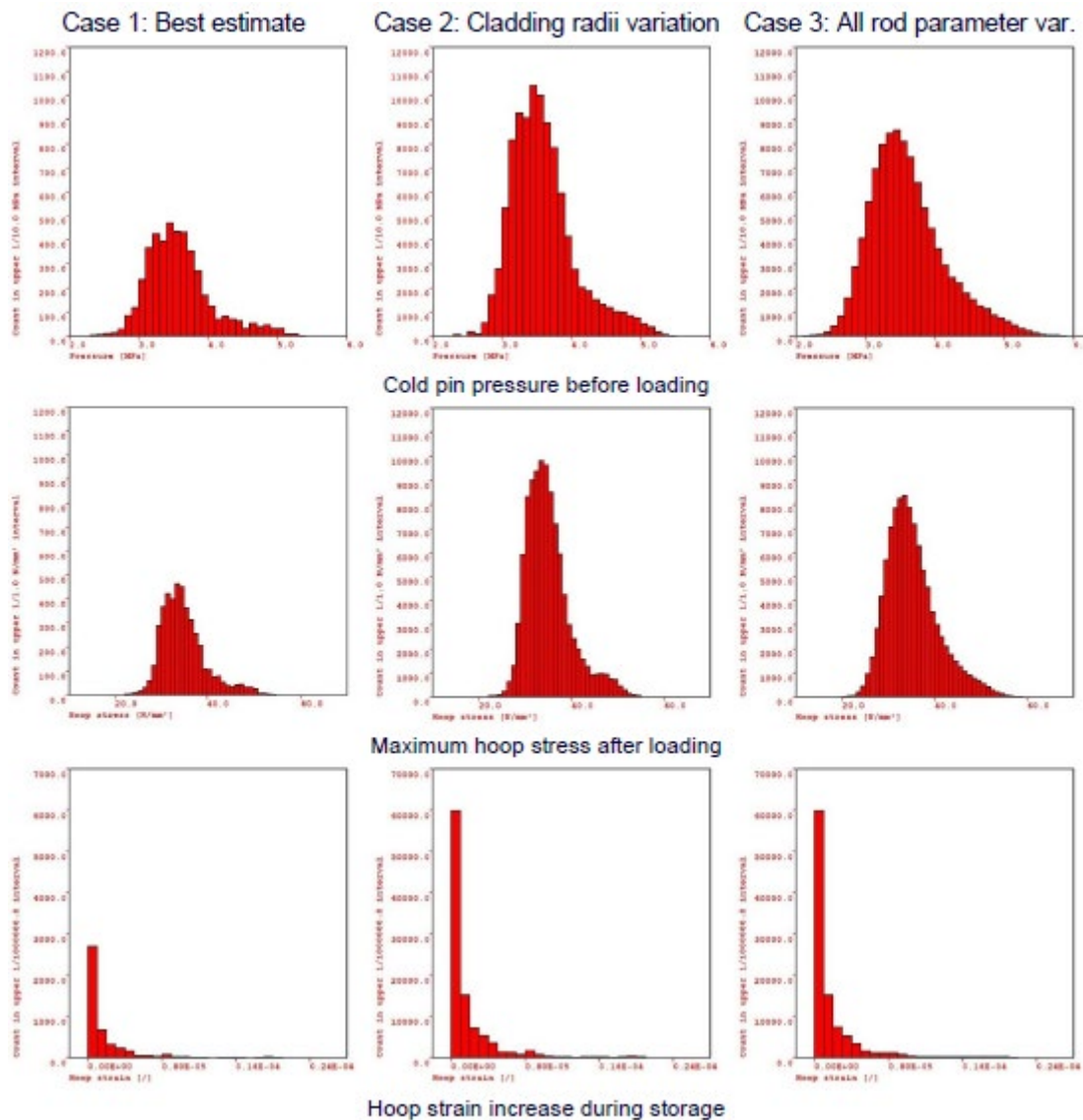


**Fig. 6** Distributions of cold inner pin pressure, cladding hoop stress and cladding hoop strain increase for three calculation cases during 100 years of dry storage (© TÜV NORD EnSys GmbH Co.KG)

These calculations give a first idea on the relevant parameter for the cladding integrity during a prolonged storage and shows the conservatism of the method used today. In the next steps the sensitivity of the inner and outer parameter on the results will be in focus.

## References

- [1] K. Lassmann, TRANSURANUS: a fuel rod analysis code ready for use, Journal of Nuclear Materials 188 (1992), 295 – 302

- [2] P. Van Uffelen, Cs. Gyóri, A. Schubert, J. van de Laar, Z. Hozer, G. Spykman, Extending the application range of a fuel performance code from normal operating to design basis accident conditions, *Journal of Nuclear Materials*, 383 (2008), 137 – 143
- [3] TÜV NORD EnSys Hannover GmbH & Co. KG, TITANIA, Data Management System for Full Core LOCA Analysis using TRANSURANUS, AESJ Water Reactor Fuel Performance Meeting, 2005, Kyoto, Japan
- [4] Extended Storage of Spent Nuclear Fuel in Casks, Inventory Assessment using Fuel Rod Performance Codes, Gerold Spykman, TÜV NORD EnSys GmbH & Co.KG, Presentation at SEDS in May 2023 at GRS in Garching, Munich
- [5] ]Entsorgungskommission – ESK, Verlängerte Zwischenlagerung bestrahlter Brennelemente und sonstiger hochradioaktiver Abfälle in Abhängigkeit von der Auswahl des Endlagerstandorts, Positionspapier vom 23.03.2023, [https://www.entsorgungskommission.de/sites/default/files/reports/ESK\\_Positionspapier\\_verlaengerte\\_ZL\\_40plus\\_ESK105\\_23032023.pdf](https://www.entsorgungskommission.de/sites/default/files/reports/ESK_Positionspapier_verlaengerte_ZL_40plus_ESK105_23032023.pdf)

**2.6 Spent Fuel Safety Analysis during Dry Storage through Fuel (GIFT) and Thermal analysis (COBRA-SFS) Integrated Code**

*Chansoo Lee, Dahyeon Woo, Changhyun Jo, Youho Lee*

*Seoul National University (SNU), South Korea*

N/A

## 2.7 Structural Response of Reinforced Concrete Structures under Impact Loading

*Lars Heibges, Hamid Sadegh-Azar*

*University of Kaiserslautern-Landau (RPTU), Germany*

### Introduction

Reinforced concrete (RC) protective walls, in particular those of nuclear or industrial installations, must be protected against unintentional or intentional impact scenarios such as aircraft crashes. In the worst-case scenario of an aircraft crash, local and global damage is caused to the structure. For a better understanding of the damage mechanisms, experimental tests as well as analytical and numerical models can be investigated. Based thereon the damage can be quantified and design guidelines developed.

The load-bearing capacity of RC slabs can be estimated by various methods and models. On the one hand, there are empirical and semi-empirical models which allow a fast calculation with few input parameters. On the other hand, validated Finite Element (FE) simulation models allow further investigation of damage mechanisms as well as detailed evaluation of stresses and strains in concrete and reinforcement.

### Empirical formulae

The perforation potential of a hard projectile and the resistance of the component are critical parameters to be taken into account in the design of reinforced concrete (RC) structures. There are already numerous empirical approaches and formulas available to calculate the required thickness of the structure to prevent perforation (see table 1) [15]. Especially in the field of nuclear engineering, some of them have been particularly established in research projects and are established in international guidelines and standards [2 – 5].

In the formulae,  $M$  and  $D$  represent the projectile's mass and diameter,  $t_d$  the plate thickness,  $V_p$  the perforation velocity,  $\rho_c$  and  $f_c$  the concrete density and compressive strength,  $N$  the nose shape factor,  $r$  the ratio of the considered reinforcement,  $\gamma$  a factor for steel layers and  $\alpha_c$  a reduction factor.

Table 1: Selected empirical formulae for perforation resistance

<b>CEA-EDF</b>	$t_p = 0.82 \cdot \frac{M^{\frac{1}{2}} \cdot V_p^{\frac{3}{4}} \cdot D}{\rho_c^{\frac{1}{8}} \cdot f_c^{\frac{3}{8}} \cdot D^{\frac{3}{2}}}$	<b>RCC-CW</b>	$t_p = \left( \frac{M}{\rho \cdot D} \cdot \left( \frac{1}{1.89} \cdot \left( \frac{\rho \cdot V_p^2}{10^6 \cdot f_c} \right) \right)^{\frac{3}{4}} \right)^{\frac{1}{2}}$
<b>CEA-EDF Fullard</b>	$t_p = \left( \frac{V_p^{\frac{1}{2}}}{1.3 \cdot \rho_c^{\frac{1}{6}} \cdot f_c^{\frac{1}{2}} \cdot \left( \frac{D}{M} \right)^{\frac{2}{3}} \cdot (r + 0.001)} \right)^2$	<b>RCC-Extended</b>	$t_p = \left( \frac{V_p^2}{1.9 \cdot f_c \cdot \rho^{\frac{1}{3}} \cdot \left( 0.35 \cdot \left( \frac{r}{200} \right)^{\gamma} + 0.65 \right)} \cdot \sqrt{\frac{M}{D}} \right)^{\frac{1}{2}}$
<b>NDRC</b>	$t_p = \alpha_p \cdot D \cdot \left( 2.2 \cdot \frac{x_c}{\alpha_c \cdot D} - 0.3 \cdot \left( \frac{x_c}{\alpha_c \cdot D} \right)^2 \right)$	<b>CRIEPI</b>	$t_p = 0.9 \cdot \left( \frac{61}{v_p} \right)^{\frac{1}{4}} \cdot \left( \frac{M \cdot V_p^2}{D \cdot f_c} \right)^{\frac{1}{2}}$
<b>De-geen</b>	$G = \alpha_c \cdot 3.8 \cdot 10^5 \cdot \frac{N \cdot M}{D \cdot \sqrt{f_c}} \cdot \left( \frac{V_p}{D} \right)^{1.8}$ $x_c = 2 \cdot D \cdot G^{0.5} \text{ für } \frac{x_c}{D} \leq 2$	<b>Chang</b>	$t_p = \left( \frac{61}{V_p} \right)^{\frac{1}{4}} \cdot \left( \frac{M \cdot V_p^2}{D \cdot f_c} \right)^{\frac{1}{2}}$

### CEB model according to Schlüter

The CEB-model according to Schlüter [20] and CEB [17] is considered a useful and simplified solution for estimating the load-bearing capacity of reinforced concrete plates subjected to soft missile impact. This analytical model describes all relevant mechanisms in a physically adequate manner and allows a fast evaluation of the system response under missile impact. The reinforced concrete plate is represented as a two-degree of freedom (TDOF) system with the following equations of motion (see equations (1) and (2), figure 1).

$$M_1 \cdot \ddot{w}_1 + c_1 \cdot \dot{w}_1 + R_1(w_1) - R_2(u) - c_2 \cdot \dot{u} = 0(1)$$

$$M_2 \cdot \ddot{w}_2 + c_2 \cdot \dot{u} + c_3 \cdot \dot{w}_2 + R_2(u) - F(t) = 0(2)$$

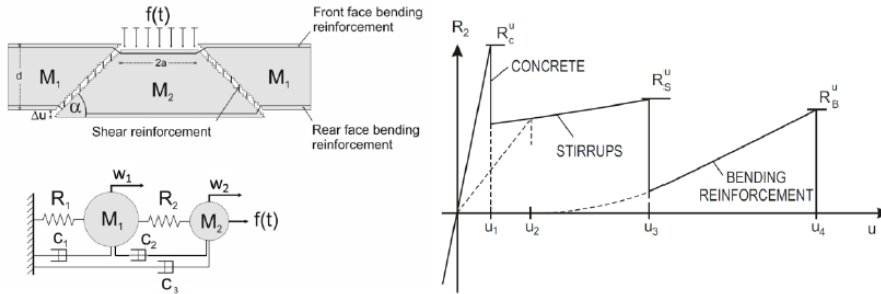


**Fig. 1** CEB model and the three components of local resistance  $R_2$  [21]

If only non-deformable parts of a plane or engine are investigated, the interaction between the target and the impacting projectile as well as the process of penetration of the projectile need to be considered. The modifications to the model are described in detail in [21].

### Numerical simulations

The verification process of numerical simulations is crucial. It is advisable to carry out a preliminary analysis using verified engineering tools (e.g. empirical formulae, CEB model) before conducting the numerical simulation. In addition, the modelling approach should be calibrated using representative experimental results. 3D fully coupled analysis is conducted, wherein the concrete is modeled using volume elements and the reinforcement bars are represented by discrete beam elements connected to the concrete's element nodes (see **Figure 2**).

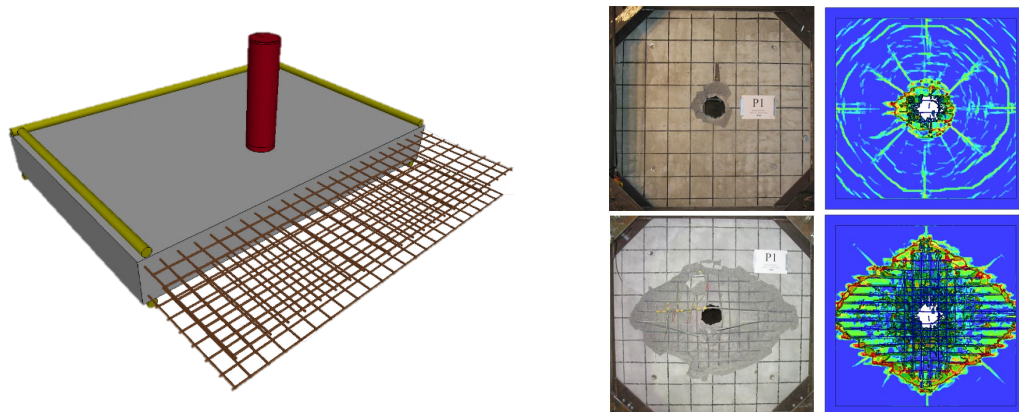


**Fig. 2** Numerical model (left) and comparison if test and simulation results for IRIS P1

Investigations concerning influence of the impact angle on the load-bearing capacity can be found in [22]. For punching tests, the damage mode is not sensitive to the implemented friction law.

### **Buried structures**

For buried structures or structures with protective layers of soil, it is essential to quantify the protective effect of the soil. Current methods for damage simulation mostly rely on empirical formulae. The application of selected empirical formulae to experimental data is elaborated in [23]. In addition, a combined numerical solution of discrete-element method for the soil and finite-element method for the projectile and concrete is presented. The diagram in Figure 3 provides an overview of the calculated penetration depth of projectiles into various soil types as a function of impact velocity.

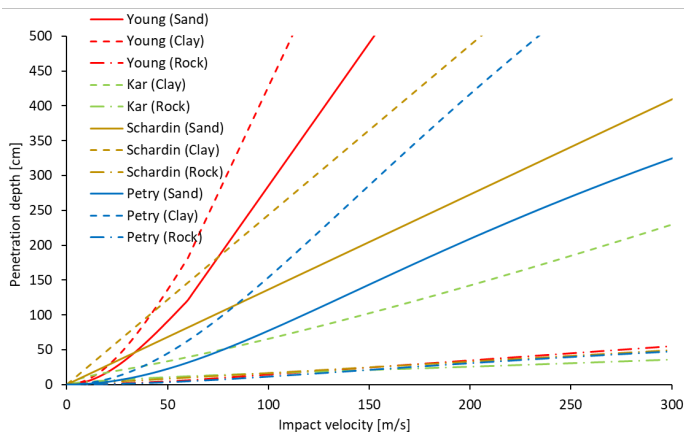


**Fig. 3** Application of the empirical formulas as a function of the impact velocity

### Acknowledgement

The work has been performed within the framework of Nuclear Safety Research Program of the German Federal Ministry for the Environment, Nature Conservation, Nuclear Safety and Consumer Protection (BMUV).

### References

- [1] Li, Q. M., Reid, S. R., Wen, H. M., Telford, A. R.: "Local impact effects of hard missiles on concrete targets". International Journal of Impact Engineering 32 (2005), S. 224–284.
- [2] Nuclear Energy Institute (2011): Methodology for Performing Aircraft Impact Assessment for New Plant Designs. Washington DC.
- [3] Comité Euro-International du Béton (1988): Concrete Structures Impact and Impulsive Loading – Bulletin D'Information.
- [4] Federal Agency of Nuclear Control (2012): Design and construction rules for nuclear power generating stations. EPR Technical Code for Civil Works ETC-C.
- [5] RCC-CW (2018). RCC-CW 2018 Edition – Rules for Design and Construction of PWR Nuclear Civil Works, AFCEN.
- [6] Schlüter, F. H. (1987). "Dicke Stahlbetonplatten unter stoßartiger Belastung – Flugzeugabsturz", PhD thesis, University of Karlsruhe, Germany.
- [7] Distler, P., Sadegh-Azar, H., Heckötter, C. (2021). "Enhancement of engineering models for simulation of soft, and hard projectile impact on reinforced concrete structures", Nuclear Engineering and Design, Volume 378.

- [8] Heibges, L.; Sadegh-Azar, H. (2023): Inclined Projectile Impact for Hard Missiles on Reinforced Concrete Slabs, TINCE 2023, Paris.
- [9] Heibges, L.; Sadegh-Azar, H. (2024): Methods for Estimating Penetration Depths and Quantification of the Protective Effect of Soil in the Event of Projectile Impact, 27th SMIRT Conference, Yokohama, Japan.

## 2.8 Evaluation of load scenarios for Spent Fuel Assemblies

*Kai Simbruner, Johannes Nicol, Tobias Grelle, Florian Rowold*

*Gesellschaft für Anlagen – und Reaktorsicherheit (GRS) gGmbH, Germany*

The project investigates handling scenarios of spent nuclear fuel (SNF) assemblies focusing on the additional loads these scenarios impose. Key scenarios include vibrations and shocks during transport (via rail, ship, road) and cask drop scenarios during handling from small heights without impact limiters. The study aims to identify effective modeling strategies using both analytical and numerical approaches, with a primary focus on finite element analyses (FEA), to simulate these conditions and build expertise.

Two primary analytical approaches were used: Beam bending analysis evaluates the deflection of fuel rods between spacer grids. Experimentally measured accelerations were converted to equivalent static loads and the largest deflection was calculated as the maximum dynamic response of the beam. Considering the resulting beam deflection, consequential contact stress analysis used Hertzian theory to calculate the contact stress between two touching fuel rods.

A variety of numerical modeling approaches were utilized. The Multibody System (MBS) considers a body-mass-spring-damper system representing the components and their interactions within the cask. The model includes the cask, primary lid, basket, and fuel elements, and simulates container drops through initial conditions. The MBS simplifies the interaction between components within the cask, yielding a system of coupled ordinary differential equations to model deformation properties and component coupling. The approach allows for sensitivity studies on the gaps and distances between components, essential for understanding the response of the system to different transport conditions. The finite element model of a single fuel rod, an Ansys Mechanical model using implicit FEA, simulates the interaction between the pellet and cladding, employing various element types (beam, shell, solid). Additionally, modal analyses were performed to determine the influence of connection modeling on the eigenfrequencies of the system.

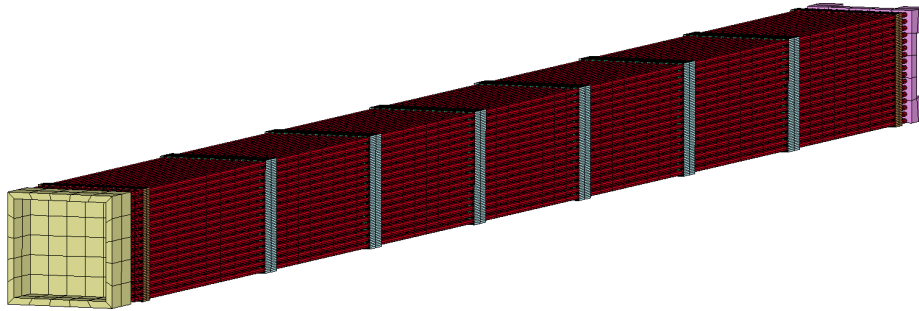


**Fig. 4** LS-Dyna FEA model of a SNF assembly

The SNF assembly finite element model aims to simulate the mechanical behavior of a spent fuel assembly using LS-Dyna for explicit FEA. The approach was derived from a series of models developed at Pacific Northwest National Laboratory /ADK 13/, /KLY 20/, and was used for simulating drop tests, shaker tables, and seismic loads. The development process involves mesh generation using a Python code which reads, manipulates, and writes LS-Dyna keyword files. This code generated the mesh based on input parameters such as fuel rod dimensions, guide tube positions, and spacer grid details. Set creation and boundary conditions were handled using LS-PrePost. Fuel rods were modeled using beam elements with a circular cross-section representing the cladding diameter. Combined density, elasticity, and bending stiffness properties were assigned to the fuel rods to simulate the cladding and fuel combined behavior. Guide tubes were modeled as tubular cross-sections. The model used 2 beam elements per spacer grid and 8 beam elements between spacer grids. Spacer grids were modeled using shell elements with rectangular cross-sections. The thickness varied according to position (inside/outside) and material (Zircaloy-4/Inconel). Spacer grids were connected to the rods using spring elements, with 6 springs per rod per spacer grid (2 springs and 4 dimples). The springs and dimples had nonlinear elastic stiffness characteristics for each material type. Top and bottom nozzles were modeled with solid elements. A tied node-to-surface approach was used to connect guide tubes and nozzles. The basket cell was modeled with rigid shells, and its prescribed motion was derived from video analysis of a 30 cm assembly drop, accounting for vertical displacement and small rotation. General contact was defined for all components to handle interactions within the assembly. Gravitational acceleration was applied to all parts of the assembly.

Preliminary results indicate qualitative effects such as buckling of the grid structure and rod-to-rod contacts. Future improvements to the SNF FEA model will focus on enhancing element types and sizes to improve time step accuracy, better understanding damping

and spring properties, and conducting comprehensive gap sensitivity studies. Validation efforts will include comparing analytical and numerical approaches. The aim is to apply these modeling techniques to various fuel element configurations and simulate a broader range of scenarios, including accidents and transport conditions.

## References

- [1] Adkins, H., Geelhood, K., Koeppel, B., Coleman, J., Bignell, J., Flores, G., Wang, J.-A., Sanborn, S., Spears, R., Klymyshyn, N.: Used Fuel Disposition Campaign, Used Nuclear Fuel Loading and Structural Performance under Normal Conditions of Transport—Demonstration of Approach and Results on Used Fuel Performance Characterization. U.S. Department of Energy (DOE), FCRD-UFD-2013-000325, 2013.
- [2] Klymyshyn, N., Kadooka, K., Ivanusa, P., Spitz, C., Fitzpatrick, J.: 30 cm Drop Modeling, Spent Fuel and Waste Disposition. Hrsg.: Department of Energy, PNNL, 2020

## 2.9 Impact of Modeling Assumptions on Muon Scattering Images of Loaded Dry Storage Casks,

*Julia Niedermeier*

*Technische Universität München (TUM), Germany*

Using cosmic muons [1] allows a non-invasive imaging of nuclear fuel in dry storage casks. The cosmic particles are investigated before and after passing through the cask. Their scattering data is then used to obtain details about the inside of the cask [2,3]. The effective scattering angles of muons depend on the properties of the interacting material. They are primarily influenced by the density and the atomic number ( $Z$ ) [4] and allow to draw conclusions about the material and geometric composition of the casks' inventory [5]. Since the fuel stored in the cask significantly differs from the surrounding materials, in terms of its density and atomic number, the resulting scattering distribution differs in that region. Consequently, the stored spent fuel can be visualized.

This study evaluates the impact of modelling assumptions and simplifications on the scattering angle distribution of muons passing through a CASTOR® V/19 cask [6,7], a standard storage cask for spent nuclear fuel. Simulations were conducted using the GEANT4 toolkit, with four cask models of varying levels of detail to assess how different simplifications affect the scattering data. The reference model is a highly accurate representation of the CASTOR® V/19 cask, incorporating detailed geometric components such as fuel assemblies, trunnions, and moderator rods. Simplified models were also created: one with homogenized moderator rods, another without trunnions or cooling fins, and a third combining both simplifications (Compare Fig.1).

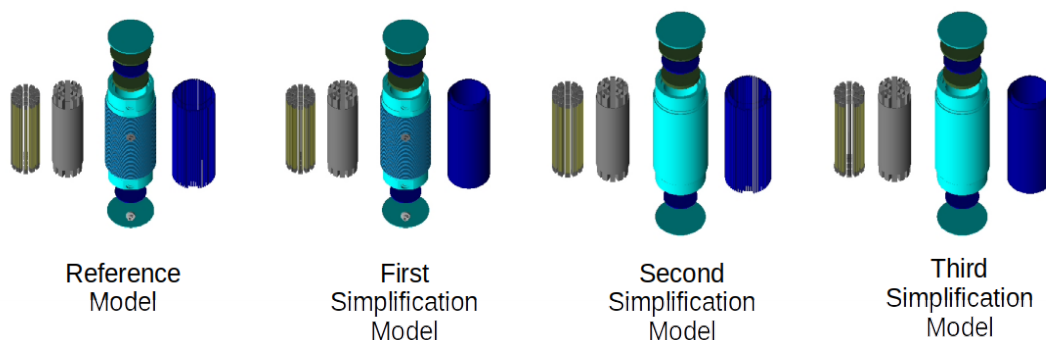


**Fig. 1** Used models for the comparative analysis.

The primary objective is to evaluate the influence of model accuracy on muon scattering distributions and identify the level of simplification at which significant changes in

scattering behaviour occur. Simulations were performed using ideal boundary conditions like ideal detectors or muons with a constant energy of 4 GeV and an incident angle of 0°. The simulations involved 4.5 million and 15 million muons.

Statistical analysis was performed using hypothesis testing, with the null hypothesis stating no significant variation in scattering data between the simplified models and the reference model. The Anderson-Darling test [8], sensitive to changes in the tails of distributions, the Kolmogorov-Smirnov test [9], effective in detecting changes in the mean, and Kuiper's test [10], ideal for identifying changes in variance, were employed to evaluate the results.

Findings reveal that simplifications can significantly impact muon scattering behaviour [11]. Even minor changes, such as homogenizing polyethylene rods (first and second simplification model), can produce substantial effects, while removing trunnions and cooling fins had negligible impact unless combined with other simplifications (second simplification model). The study concludes that careful assessment of the level of simplification in models is crucial to ensuring the precision and reliability of muon scattering results. Simplifications should be chosen judiciously to avoid statistically significant influences on the outcome [11].

## References

- [1] Seth H. Neddermeyer and Carl D. Anderson. "Note on the Nature of Cosmic-Ray Particles". In: *Physical Review* 51.10 (1937), pp. 884–886. ISSN: 0031-899X. DOI: 10.1103/PhysRev.51.884.
- [2] Tanaka, H.K.M., Bozza, C., Bross, A. et al. Muography. *Nat Rev Methods Primers* 3, 88 (2023). <https://doi.org/10.1038/s43586-023-00270-7>
- [3] Konstantin N. Borozdin et al. "Radiographic imaging with cosmic-ray muons", in: *Nature* 422.6929, 2003, p. 277. ISSN: 0028-0836., DOI:
- [4] Gerald R. Lynch and Orin I. Dahl. "Approximations to multiple Coulomb scattering". In: *Nuclear Instruments and Methods in Physics Research Section B: Beam Interactions with Materials and Atoms* 58.1 (1991), pp.6–10. ISSN: 0168583X. DOI: 10.1016/0168-583X(91)95671-Y.
- [5] L. J. Schultz et al., "Statistical Reconstruction for Cosmic Ray Muon Tomography," in *IEEE Transactions on Image Processing*, vol. 16, no. 8, pp. 1985-1993, Aug. 2007, doi: 10.1109/TIP.2007.901239.
- [6] Product Info Castor® V/19. GNS Gesellschaft für Nuklear-Service mbH

- [7] GNS. URL: <https://www.gns.de/behaelter-equipment/brennelemente-haw/castor/> (visited on 08/02/2024).
- [8] T. W. Anderson and D. A. Darling, "A Test of Goodness of Fit," *Journal of the American Statistical Association*, 49, 268, 765 (1954)URL <http://www.jstor.org/stable/2281537>.
- [9] M. A. Stephens, "Use of the Kolmogorov-Smirnov, Cramer-Von Mises and Related Statistics Without Extensive Tables," *Journal of the Royal Statistical Society. Series B (Methodological)*, 32, 1, 115 (1970)URL <http://www.jstor.org/stable/2984408>.
- [10] N. H. Kuiper, "Tests concerning random points on a circle," *Nederl. Akad. Wetensch. Proc. Ser. A*, vol. 63, 38–47 (1960).
- [11] Niedermeier J. and Stuke. M, "Impact of Modeling Assumptions on Muon Scattering Images of Loaded Dry Storage Casks", accepted for publication in *Nuclear Science and Engineering*.

**2.10 Radiation-based methods for non-invasive monitoring of transport and storage casks**

*Suzanne Eisenhofer, Michael Wagner, Uwe Hampel*

*Technische Universität Dresden (TUD), Germany*

N/A

## 2.11 Update of the SPIZWURZ project

*Sarah Weick, Mirco Große, Conrado Roessger, Juri Stuckert*

*Karlsruher Institut für Technologie (KIT), Germany*

Internal and external stresses affect zirconium based cladding tubes throughout their slow cooling during interim dry storage. Generally, hydrogen in solid solution follows gradients in temperature, concentration, and stress. Consequently, hydrogen moves from higher to lower temperatures and from lower to higher stresses due to the thermodynamic more favourable conditions. The influence of an applied elastic tensile stress on the hydrogen solubility and diffusion is investigated as a part of the SPIZWURZ project. This project was initiated as a cooperation between the Gesellschaft für Anlagen- und Reaktorsicherheit (GRS) and the Karlsruhe Institute of Technology (KIT) in Germany. In the project the flow and the chemical potential of hydrogen in cladding tube materials shall be determined under conditions of long-term interim dry storage of spent fuel elements in transport and storage casks.

In this framework, a long-term bundle test at the KIT's LICAS facility was conducted for 250 days, from the 12th May 2023 until the 17th January 2024. 21 cladding tubes out of three different alloys were therefore depicted with either 100 wt.ppm or 300 wt.ppm of hydrogen and either an inner gas pressure of 106 or 146 bar. Before and after the hydrogenation of the cladding tubes, their diameter was measured by a laser scanner, in order to quantify the amount of hydrides in the bulk after the hydrogenation, as shown in Fig. 1 for a ZIRLO and a Zry-4 cladding tube that were hydrogenated with 300 wt.ppm of hydrogen at a temperature of 450°C.

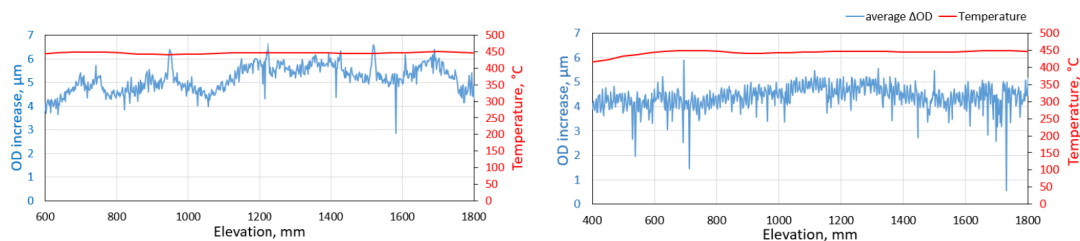


**Fig. 1** Laser scan measurements of the change in the outer diameter  $od$  along the axial positions after the hydrogenation with 300 WT.PPM hydrogen of the central part of a zirlo (left) and a ZRY-4 cladding tube (right)

After heating up the bundle to a maximum temperature of 409°C at the central rod (rod 1), a uniform cooldown process of 1K/day was started and is visualised in Fig. 2 for three thermocouple positions within the bundle at the hottest zone.

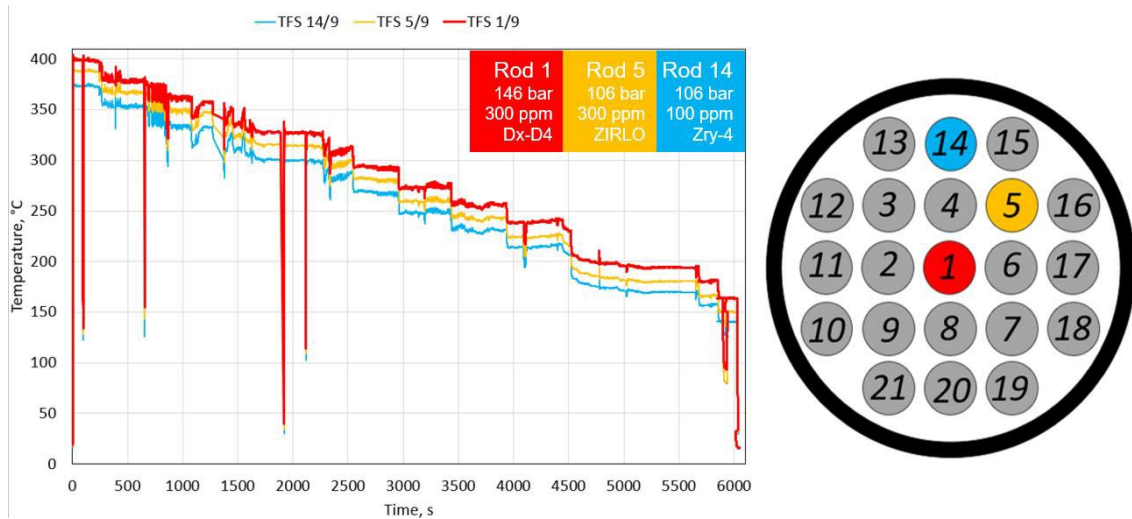


**Fig. 2** Temperature history of rod 1, 5 and 14 at the hottest zone (left) and corresponding scheme of the bundle cross section (right)

Following analysis via metallography, carrier gas hot extraction (CGHE) and neutron imaging are in progress.

## 2.12 **SPIZWURZ Benchmark for simulation of hydrogen behaviour in fuel rod claddings at dry storage relevant conditions. Phase 1 (Blind tests)**

*Aleksandra Rezchikova*

*Gesellschaft für Anlagen – und Reaktorsicherheit (GRS) gGmbH, Germany*

The assessment of the fuel integrity during the entire storage period is an important safety aspect and relies strongly on numerical simulations since the experimental data is very limited. Moreover, the real dry storage conditions can be reproduced by the experiments only to a certain extent, taking into account the storage duration and the safety issues associated with the use of irradiated materials. For these reasons, the development of decent numerical tools is of great importance.

Hydrogen-related effects are supposed to be among the main fuel rod degradation mechanisms during long-term dry storage and are still not well understood. The collaborative project SPIZWURZ between the Karlsruhe Institute of Technology (KIT) and the Gesellschaft für Anlagen- und Reaktorsicherheit (GRS) was thus initiated to investigate hydrogen behaviour in fuel rod cladding tubes at microscopic and macroscopic scales during a long-term interim dry storage of spent nuclear fuel in transport and storage casks.

Within the frame of the SPIZWURZ project, a slow cool-down experiment of a fuel rod simulator bundle with pre-hydrogenated non-irradiated cladding tubes was conducted at the KIT-QUENCH facility. After the maximum cladding temperature within the bundle attained the value of 405°C, the bundle was cooled over 8 months with a maximum average rate of 0.94 °C/day. A scheme of the bundle cross-section is shown in **Figure 5**. The SPIZWURZ Bundle Test matrix includes 3 cladding materials (Zircaloy-4, opt. ZIRLO and Duplex Dx/D4), 2 pressurization levels (103 bar and 142 bar), and 2 target hydrogen concentrations (100 wppm and 300 wppm).

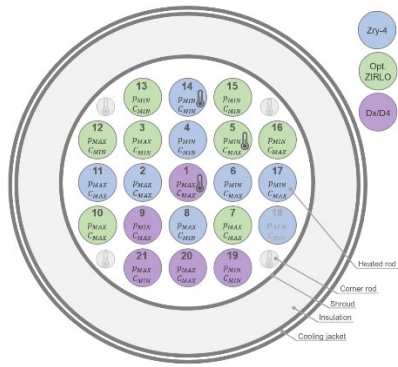


**Fig. 5** SPIZWURZ test bundle (top view)

The subsequent analysis of the cladding tubes aims to determine a creep behaviour of the cladding tubes and parameters that describe the hydrogen diffusion and solubility under conditions relevant to dry storage. The obtained experimental results provide a basis for the SPIZWURZ Benchmark, which aims to validate and improve hydrogen behaviour modelling in the existing fuel performance codes. The SPIZWURZ Blind Benchmark, coordinated by the GRS, started in April 2024 and will finish at the end of September 2024.

## 2.13 Evaluation methodology of spent fuel mechanical performance under $\text{UO}_2$ oxidation in dry management

*Francesco Feria, Carlos Aguado, Luis E. Herranz*

*Centro de Investigaciones Energéticas, Medioambientales y Tecnológicas (CIEMAT), Spain*

### Introduction

The safety of spent nuclear fuel during dry management requires preserving the cladding integrity as the first containment barrier for fission products. Various phenomena can degrade the fuel cladding during storage, increasing its failure probability. Among them, the oxidation of the fuel matrix ( $\text{UO}_2$ ) could induce cladding failure, as noted by ISG-22 (USNRC, 2006).

A scenario involving cladding integrity loss due to pellet oxidation under the thermal conditions of a dry unloading requires an undetected defect in the cladding and an oxidizing agent contacting the fuel through the defect. Under these conditions, the transformation of  $\text{UO}_2$  to  $\text{U}_3\text{O}_8$  in sufficient magnitude would result in a volume increase. The resultant circumferential stress on the cladding could propagate the defect and lead to failure. The interest in the defect propagation initiation time is discussed in ISG-22 (USNRC, 2006), which proposes using time-temperature (t-T) curves as a safety criterion.

Previous collaborations between CIEMAT and ENRESA derived a correlation for cladding failure propagation time as a function of temperature and burnup, based on experimental data available in the literature for irradiated rods subjected to unlimited oxidation (Feria and Herranz, 2008; Herranz and Feria, 2009). Earlier, t-T curves were derived by Hanson (2000), but they were based on the oxidation of irradiated pellet fragments with an unlimited supply of oxidant and without the presence of cladding

The mentioned t-T curves are limited to low burnup ( $< 45 \text{ GWd/tU}$ ) and do not analyze the effect of  $\text{O}_2$  partial pressure. Additionally, the database for the most comprehensive t-T curves (based on experiments with cladding) is limited and scattered in the literature. Meanwhile, t-T curves based on pellet fragment oxidation, though better supported experimentally, require thermo-mechanical calculations considering the gap (if open) and mechanical interaction with the cladding. No analytical methodologies using thermo-mechanical codes exist to evaluate cladding deformation and potential failure due to pellet oxidation to  $\text{U}_3\text{O}_8$ .

Thus, this work aims to develop a methodology for evaluating cladding failure due to fuel oxidation, considering limited O<sub>2</sub> concentrations.

## Methodology

### Compilation of data of interest

Data from the High Activity Waste Unit of CIEMAT within the OCATS project (Unirradiated UO<sub>2</sub> oxidation tests and associated analyses) with ENRESA were used (Milena-Pérez et al., 2020; Milena-Pérez, 2023a). These experiments utilized powder from unirradiated pellets, oxidizing them at different partial pressures of O<sub>2</sub> (Milena-Pérez, 2023a).

### Selection and extension of the t-T curves

Two types of t-T curves was identified in the literature, based on different experimental approaches: integral experiments with irradiated rods and local experiments with pellet fragments.

The CIEMAT-derived t-T curves determine the incubation time,  $t_{inc}$  (h), as a function of fuel temperature, T (K), and average burnup, Bu (GWd/tU):

$$t_{inc} = 1.54 \cdot Bu^{-7.075} \cdot \exp\left[\frac{-723.44 + 5235.38 \cdot \ln(Bu)}{T}\right] \quad (1)$$

These curves are valid for a temperature range relevant to dry storage (200-400°C) but are constrained to a narrow range of low burnups (8-27 GWd/tU) and do not account for limited O<sub>2</sub> partial pressures during oxidation (Milena-Pérez, 2023a; Milena-Pérez, 2023b).

The PNNL formulation provides an alternative approach where  $t_{inc}$  (h) is derived as the sum of times for complete formation of U<sub>4</sub>O<sub>9</sub> ( $t_{100\%U4O9}$ ) and the transformation from U<sub>4</sub>O<sub>9</sub> to U<sub>3</sub>O<sub>8</sub> ( $t_{100\%U4O9 \rightarrow 100\%U3O8}$ ):

$$t_{inc} = t_{100\%U4O9} + \lambda \cdot t_{100\%U4O9 \rightarrow 100\%U3O8} \quad (2)$$

$$t_{100\%U4O9} = 1.4 \cdot 10^{-8} \exp\left(\frac{105000}{R \cdot T}\right) \quad (3)$$

$$t_{100\%U4O9 \rightarrow 100\%U3O8} = 4.84 \cdot 10^{-14} \exp\left(\frac{150000 + 10^3 Bu}{R \cdot T}\right) \quad (4)$$

This model considers local burnup from pellet fragment experiments and incorporates a factor  $\lambda$  to adjust for  $U_3O_8$  formation triggering cladding propagation. The PNNL curves are established under 21%  $O_2$  and within a specific temperature range (255-325°C). The local burnup range extends from 16 to 42 GWd/tU (Hanson, 2000).

In this work, the PNNL formulation was selected due to its alignment with experimental data from CIEMAT's High Activity Waste Unit. Non-irradiated pellet powder was oxidized under varying  $O_2$  partial pressures to extend the t-T curves. Using a thermo-mechanical code instead of  $\lambda$ , the work focuses on  $t_{100\%U_3O_8}$  as the key metric.

Figure 1 compares PNNL's t-T curves with data from the OCATS project for the total formation of  $U_3O_8$ , noting that conservative times closer to 90%  $U_3O_8$  formation were used. OCATS experimental data with 1%  $O_2$  nearly match the PNNL curve for 21%  $O_2$  at 16 GWd/tU burnup. Although direct temperature trend comparison is difficult due to limited range overlap, OCATS data appear to follow PNNL's temperature trend. OCATS data indicate a non-linear, potentially exponential, relationship between analyzed time and burnup. The impact of reducing  $O_2$  concentration from 10% to 1% on increasing the analyzed time is similar to the effect of burnup up to 16 GWd/tU but becomes negligible between 21% and 10%.

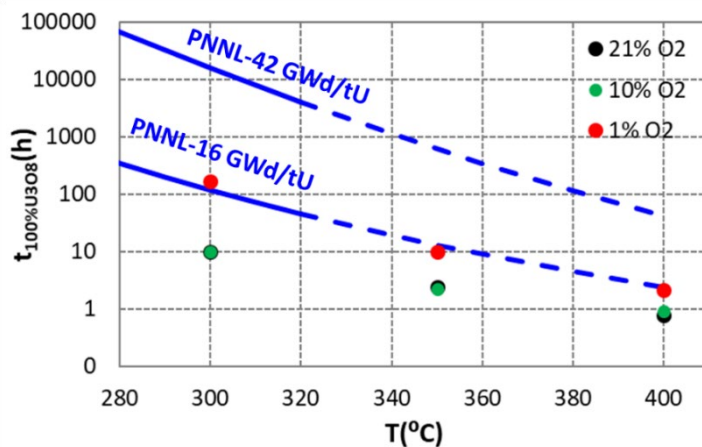


**Fig. 1** Total formation time of  $U_3O_8$  as a function of temperature for various burnups (lines corresponding to PNNL t-T curves valid for 21%  $O_2$ ; dashed lines indicate extrapolation beyond temperature validity range) and different partial oxygen concentrations (points corresponding to OCATS experiments with non-irradiated material).

### Adaptation of FRAPCON-xt

The derived methodology in this work uses the thermo-mechanical tool FRAPCON-xt (Feria et al., 2015; Feria et al., 2020), an extension of the FRAPCON code developed by PNNL (Geelhood et al., 2015) to dry storage conditions.

FRAPCON-xt, incorporates thermal characterization during storage. This characterization was derived from 3D calculations using FLUENT (Feria et al., 2015; Herranz et al., 2015). It also includes a semi-empirical cladding creep law designed for dry storage conditions (Herranz and Feria, 2010) and a hydrogen migration/precipitation/reorientation model in cladding known as HYDCLAD (Feria and Herranz, 2018; Feria et al., 2020), which is applicable both in dry storage and irradiation scenarios.

FRAPCON-xt does not include fuel pellet oxidation. Developing a phenomenological oxidation model would require unavailable information and involve significant uncertainties. However, the current FRAPCON-xt formulation can incorporate a t-T curve-based model, where specified conditions result in mechanical loading on the cladding due to  $U_3O_8$  formation. The following hypotheses and approximations have been applied for the conservative adaptation of FRAPCON-xt:

- Unlimited oxidant supply.
- Uniform pellet oxidation along the azimuth.
- No volumetric change due to  $U_4O_9$  formation.
- Formation of  $U_3O_8$  (associated with the start of pellet expansion) following the total transformation of the fuel to  $U_4O_9$ , using the PNNL correlation (equation 3).
- Linear pellet deformation over time until complete  $U_3O_8$  formation (behavior observed up to approximately 90%  $U_3O_8$  formation). This deformation is added to that calculated by FRACAS-I.
- Isotropic and linear pellet deformation, equivalent to a 36% volumetric increase (Milena-Pérez, 2023a).

- O<sub>2</sub> diffusion to inner rings conditioned on the complete transformation to U<sub>4</sub>O<sub>9</sub> in the adjacent outer ring.
- Number of rings in the fuel matrix estimated by similarity with fragments used in oxidation tests (around 200 mg in Hanson (2000)).
- Height of the node to be oxidized equivalent to the diameter of the cladding defect.
- Defect propagation initiation time identified with 1% circumferential plastic deformation (Einzigler and Cook, 1985), after mechanical contact between U<sub>3</sub>O<sub>8</sub> and cladding.

#### Application of adapted FRAPCON-xt for verification

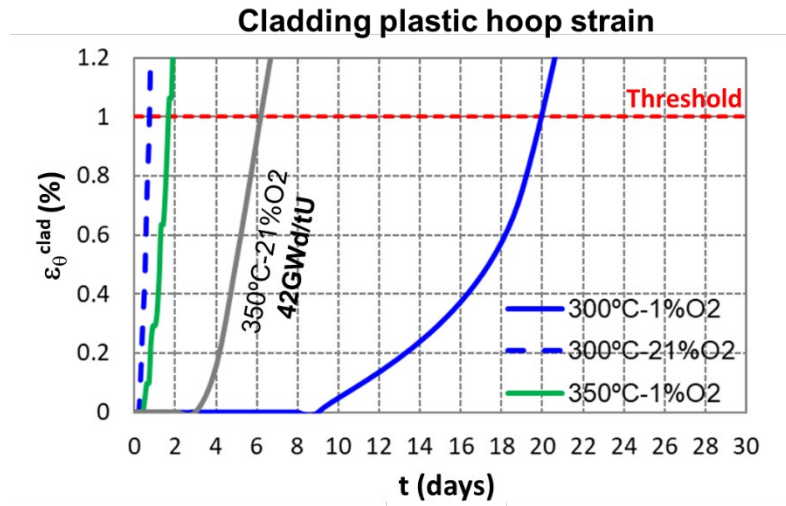
The previously described methodology was applied to a scenario involving a fuel rod with ZIRLO cladding (17x17 Modified Advanced European Fuel, MAEF), irradiated to high burnup (average burnup of the rod above 45 GWd/tU), with an undetected defect of 760 μm (Einzigler and Cook, 1985). The rod was simulated under different isothermal conditions (300, 350, and 400°C) and partial O<sub>2</sub> concentrations (1%, 10%, 21%).

Figure 2 shows the results of the permanent circumferential deformation of the cladding over time during the simulated discharge. At 400°C (at any partial O<sub>2</sub> concentration), the mechanical stress on the cladding exceeded acceptable limits in FRAPCON, making it impossible to produce any results. The same occurred at 350°C with 10% and 21% O<sub>2</sub>. These cases are inferred to result in defect propagation times of minutes at 400°C and hours at 350°C, which are shorter than the limit time obtained at 300°C and 21% (or 10%) O<sub>2</sub> (17 hours). At 350°C and 21% O<sub>2</sub>, results using the PNNL t-T curve (equation 2 with λ=1) with a burnup of 42 GWd/tU were added, showing that the significant burnup damping effect extends the defect propagation initiation time to 6 days.

The results in Figure 2 highlight the significant impact of temperature on the time at which the defect propagation starts; at 1% O<sub>2</sub>, this time limit increases from 40 hours at 350°C to 20 days at 300°C. At 300°C, the O<sub>2</sub> partial pressure effect shows a considerable sensitivity, with the limit time increasing from 17 hours at 21% (or 10%) to 20 days at 1%. Notably, choosing deformation limits higher than 1% (e.g., 2% as per Goll et al. (2001))

would yield similar initiation times due to the steepness of the curves in Figure 2 near the limit.

This application confirmed the consistency of the developed methodology.



**Fig. 2** Evolution of circumferential cladding plastic hoop strain ( $\epsilon_{\theta}^{\text{clad}}$ ) over time post-discharge for various temperatures and partial oxygen concentrations (21% also includes 10%). Results considering the PNNL t-T curve (21%  $O_2$ ,  $\lambda=1$ ) at 350°C and 42 GWd/tU are shown in gray. The red dashed line indicates the deformation threshold for the onset of defect propagation.

## Conclusions

This report presents an analytical methodology to determine the maximum time an irradiated fuel rod with an undetected defect can be exposed to an oxidizing agent ( $O_2$ ).

The methodology is based on a conservative adaptation of FRAPCON-xt to account for the oxidation phenomenon of  $UO_2$ , using the concept of t-T curves. Specifically, the t-T curves used were an extension of a selected formulation from the literature (PNNL model, consistent with experiments conducted in the OCATS project) to the conditions tested in the OCATS project (unirradiated  $UO_2$  subjected to oxidation at different partial  $O_2$  concentrations).

The consistency of this methodology was verified by applying it to a postulated scenario under isothermal conditions and atmospheres with different partial  $O_2$  concentrations. At temperatures around 300°C and in the presence of air, defect propagation would not occur until approximately 24 hours; this "incubation time" would increase to over 2 weeks

if the O<sub>2</sub> concentration were limited to around 1%. It is important to note that the estimated times are conservatively interpreted.

### **Acknowledgments**

The authors wish to thank ENRESA for the technical discussions held and the funding provided for this work.

### **References**

- [1] Einziger, R.E., Cook, J.A., 1985. Behavior of Breached Light Water Reactor Spent Fuel Rods in Air and Inert Atmospheres at 229°C. *Nuclear Technology*. 69, 55-71.
- [2] Feria, F., Herranz, L.E., 2008. Oxidación del UO<sub>2</sub> durante el almacenamiento temporal en seco. CIEMAT, DFN/SN-02/OP-08.
- [3] Feria, F., Herranz, L.E., Penalva, J., 2015. On the way to enabling FRAPCON-3 to model spent fuel under dry storage conditions: The thermal evolution. *Annals of Nuclear Energy*, 85, 995-1002.
- [4] Feria, F., Herranz, L.E., 2018. Effect of the oxidation front penetration on in-clad hydrogen migration. *Journal of Nuclear Materials*, 500, 349–360.
- [5] Feria, F., Aguado, C., Herranz, L.E., 2020. Extension of FRAPCON-xt to hydride radial reorientation in dry storage. *Annals of Nuclear Energy*, 145, 107559.
- [6] Geelhood, K.J., Luscher, W.G., Raynaud, P.A., Porter, I.E., 2015. FRAPCON-4.0: A Computer Code for the Calculation of Steady-State, Thermal–Mechanical Behavior of Oxide Fuel Rods for High Burnup. PNNL-19418, Vol.1 Rev.2.
- [7] Goll, W., Spilker, H., Toscano, E., 2001. Short-time creep and rupture tests on high burnup fuel rod cladding. *Journal of Nuclear Materials* 289(3), 247-253.
- [8] Hanson, B., 2000. Clad Degradation - Dry Unzipping. ANL-EBS-MD-000013.
- [9] Herranz, L.E., Feria, F., 2009. Spent fuel rod splitting due to UO<sub>2</sub> oxidation during dry storage: Assessment of the database. *Progress in Nuclear Energy*, vol. 51, pp. 201-206.
- [10] Herranz, L.E., Feria, F., 2010. Extension of the FRAPCON-3.3 creep model to dry storage conditions. *Progress in Nuclear Energy*, 52, 634–639.
- [11] Herranz, L.E., Penalva, J., Feria, F., 2015. CFD analysis of a cask for spent fuel dry storage: Model fundamentals and sensitivity studies. *Annals of Nuclear Energy*, 76, 54–62.
- [12] Milena-Pérez, A., Rodríguez-Villagra, N., Fernández-Carretero, S., Aguado, C., Feria, F., Herranz, L.E., 2020. Caracterización analítica del combustible nuclear. CIEMAT, DFN/RA-01/SP-20.

- [13] Milena-Pérez, A., 2023a. Oxidation of the spent nuclear fuel matrix under interim storage conditions. Tesis doctoral.
- [14] Milena-Pérez, A., Rodríguez-Villagra, N., Feria, F., Aguado, C., Herranz, L.E., 2023b. Critical review of fuel oxidation database under dry storage conditions. Progress in Nuclear Energy 165, 104914.
- [15] 49USNRC, 2006. Potential rod splitting due to exposure to an oxidizing atmosphere during short-term cask loading operations in LWR or other uranium oxide based fuel. Interim Staff Guidance – 22.

## **2.14 Investigation of chemical and mechanical properties of irradiated Zircaloy possibly influencing the structural integrity during dry (long-term) interim storage**

*Yvonne Lin, Maria Vrellou, Michael Herm, Tobias König, Arndt Walschburger, Volker Metz, Christoph Kirchlechner*

*Karlsruher Institut of Technology (KIT), Germany*

The management of spent nuclear fuel (SNF) in Germany foresees direct disposal in a deep geological repository being available after 2050. Currently, SNF assemblies, discharged from power reactors, are stored in dual-purpose casks (DPC) within interim dry storage facilities. However, delays in the site selection process mean that the licensed interim storage period and DPCs will expire before the anticipated commissioning of a final repository [1-2]. Consequently, the SNF may need to be stored in dry storage for up to a century. Understanding the mechanical and chemical properties of irradiated Zircaloy cladding and their evolution is essential to ensure the safe handling of SNF assemblies after prolonged interim dry storage.

This study focuses on examining Zircaloy-4 claddings extracted from uranium dioxide and mixed oxide fuel rod segments irradiated in commercial pressurized water reactors, during the 1980s, to average burnups of 50.4 GWd/tHM and 38 GWd/tHM respectively. Specimens were sampled from the plenum and from fuel rod segments, where the claddings are in contact with the SNF pellets. Characterization techniques including scanning electron microscopy, electron backscatter diffraction (EBSD), nanoindentation, laser scan micrometre measurements, and Synchrotron radiation-based techniques are employed to determine chemical and mechanical properties of the irradiated cladding samples. Similarly, the deposition of fission or activation products in fuel-cladding chemical interaction (FCCI) layers is also explored, because isotopes such as caesium, iodine, tellurium and chlorine can form agglomerates in a corrosive process, which may possibly affect the cladding integrity [3].

Experiments and preliminary findings at this stage primarily focus on the microstructural investigation of non-irradiated Zircaloy-4 samples, both hydrogenated and non-hydrogenated. These studies serve as precursors to subsequent experiments involving irradiated Zircaloy cladding by validating the reliability and effectiveness of the proposed methodologies in determining the crystallographic texture, influence of radiation damage, and hydride morphology of future (irradiated) cladding samples. Moreover, cladding

diameter variations due to the swelling of the pellet were measured using the laser scan micrometre before and after removal of the SNF and found to be within the uncertainty of the measurements. Analyses with various characterization techniques demonstrate that crystalline agglomerates present in FCCI layers consist of U-O-Zr-Cs-CI-I rich phases.

The next steps will involve completing the sample characterization and mechanical property investigations of irradiated cladding. Further micromechanical tests will aim to determine plastic deformation, strengthening mechanisms, and fracture behavior. Correlation of mechanical data with microstructural

observations will elucidate embrittlement mechanisms and assess the influence of long-term storage conditions on Zircaloy cladding integrity.

## References

- [1] “BGZ’s research programme: Thinking ahead interim storage” BGZ’s research programme: <https://bgz.de/2022/11/02/bgzs-research-programme-thinking-ahead-interim-storage/> (accessed Jan. 5, 2024).
- [2] V. Metz et al., “Radionuclide behaviour in the near-field of a geological repository for spent nuclear fuel,” *Radiochimica Acta*, vol. 100, no. 8–9, pp. 699–713, Aug. 2012. doi:10.1524/ract.2012.1967
- [3] T. Koenig et al. “Examination of volatile fission and activation products within the fuel-cladding interface of irradiated PWR fuel rod segments”, Workshop on Safety of Extended Dry interim Storage of SNF, Garching, 2021.

## **2.15 Activities of Axpo in the field of fuel integrity during dry storage**

*Martin Zemek*

*Axpo Power AG, Switzerland*

Axpo Nuclear is owner / shareholder of all Swiss NPPs and waste management organizations and is operator of the nuclear power plant Beznau (2xPWR) and manages the fuel cycle also for the Leibstadt power plant (BWR).

According to the Swiss law, the operators of nuclear facilities are responsible for the radioactive waste management including spent nuclear fuel [1,2]. Correspondingly Axpo operates one own intermediate storage facility at the area of the Beznau power plant ZWIBEZ, is a shareholder of the national intermediate storage facility ZWILAG and is one of the members in the National Cooperative for the Disposal of Radioactive Waste NAGRA.

Technically Axpo has to provide a concept for the management of spent fuel assemblies including a proof of integrity of the fuel rod cladding during intermediate storage as required by the ENSI guideline G20 [3]. To do so, temperature limits are to be defined for the residence in the dry storage cask [4]. Here, Axpo has licensed a deterministic conservative methodology, following the integrity criteria for the maximum local hoop stress of 120 MPa and maximum local creep strain in hoop direction of 1% at the end of dry storage. These temperature limits are defined for each fuel rod and assembly design and are also one of the boundary conditions for the licensing of the dry storage casks and for the design of individual cask inventories.

Furthermore, we are obliged by the regulation [4] to follow-up the state of the art of science and technology. As the rod failure mechanisms are continuously discussed and reviewed in national and international programs and organizations we have to review the considered boundary conditions and integrity criteria. Frequently the applicability of findings from the various research programs are requested by the regulator on an informal or formal way. Support of research is perhaps the most effective way to address such requests, where experimental results were produced using samples from our reactors. Axpo supports the SwissNuclear programs at PSI by financial aid and provision of irradiated samples. Currently, programs for investigation of hydrogen behavior and mechanical properties (NEURAL, HyMec+) are ongoing e.g. [5,6]. International programs managed by EPRI and Studsvik are supported as well financially and/or by provision of

irradiated samples. Past programs for creep testing of irradiated cladding materials and hydride re-orientation studies can be mentioned here [7]. Currently ongoing programs in the frame of NFIR, SCIP are also supported, but we are facing increasing difficulties with transport of rods or segments. The outcomes of the research are applied in engineering studies that are feasible to be performed additionally to our operative tasks, e.g. the modelling of the hydride re-distribution during the dry storage [8].

The integrity of the spent fuel assemblies during dry storage in our concept was always confirmed despite of adjustments that were necessary during the past years.

In the workshop examples of the above mentioned activities are presented.

## References

- [1] Kernenergiegesetz (KEG) 732.1
- [2] Kernenergieverordnung (KEV) 732.11
- [3] Richtlinie für die schweizerischen Kernanlagen ENSI-G20, “Reaktorkern, Brennelemente und Steuerelemente: Auslegung und Betrieb“
- [4] Richtlinie für die schweizerischen Kernanlagen ENSI-G05, „«Auslegung und Fertigung von Transport- und Lagerbehältern für die Zwischenlagerung”
- [5] Colldewei A.W. et al., Journal of Nuclear Materials 561 (2022) 153549, “Delayed hydride cracking in Zircaloy-2 with and without liner at various temperatures investigated by high-resolution neutron radiography”
- [6] Fagnoni F. et al., Journal of Nuclear Materials 584 (2023) 154574, “Hydrogen diffusion in zirconium cladding alloys with an inner liner as quantified by neutron radiography and nanoindentation”
- [7] Auzoux Q. et al., Journal of Nuclear Materials 494 (2017) 114-126, “Hydride reorientation and its impact on ambient temperature mechanical properties of high burn-up irradiated and unirradiated recrystallized Zircaloy-2 nuclear fuel cladding with an inner liner”
- [8] Zemek M. et al., ENS TopFuel 202, 1paper 79, “Effects of the liner on ductility of claddings after dry storage – a review”

## **2.16 Activities related to the characterization of spent nuclear fuels by Tractebel**

*Adrien Dethioux, Jinzhao Zhang,*

*Tractebel (ENGIE), Belgium*

### **Introduction**

In Belgium, there is no clear decision on the final disposal of spent fuels. The geological storage is the chosen option, but many aspects still need to be clarified. Moreover, it is planned to shutdown 5 of the 7 nuclear reactors by end of 2025. In that context, management of the spent fuels during long term storage becomes a priority.

This leads to various activities related to characterization of spent fuels at Tractebel, including the two that will be detailed here: The first is the participation in the IAEA Coordinated Research Project (CRP) of Spent Fuel Characterization, in cooperation with CEA, France. The second is calculation of fission gas release (FGR) at end of life for typical fuel assemblies for SYNATOM, responsible for the front and back end of nuclear fuels. The aim is to have a better characterization of the spent fuels through thermal mechanical modelling and simulation in order to ensure a safe storage of the spent fuels. It also provide useful information to SYNATOM for management of the spent nuclear fuels.

The first activity permitted to improve the simulation with FRAPCON, confirm that we had consistent results with other codes, establish a method for evaluating the parameters relevant for hydride reorientation and identify the most important contributors.

The second activity permitted to create and qualify a system to evaluate the fission gas release of spent fuel rods. It is able to treat a large number of assemblies in one run. It can be used for support studies linked to spent fuel characterization.

### **IAEA CRP on spent fuel characterization**

The contribution of Tractebel to this CRP is a benchmark of fuel performance codes for simulating the thermal mechanical behaviour of the fuel rods under irradiation in reactor and storage in dry casks. It focuses on the risks of creep and hydride reorientation. There are no experimental data, but the access to extensive operational experience is an asset.

The benchmark is based on a joint specification with the CEA in France. The fuel design is an anonymized version of a fuel assembly type used in Belgium. It is typical 17x17 12 feet fuel assemblies of pressurized water reactors. The simulated life of the assembly covers irradiation in reactor, cooling in pools, drying and cask storage up to 100 years. All the conditions are inspired by real assemblies with the aim at being realistic, without giving exact information. There are sensitivity studies covering the irradiation conditions, dry cask storage conditions, fuel design and simulation models. The code used by Tractebel is FRAPCON 4.0, and the code used by CEA is ALCYONE.

In the base case, the evolution of rod internal pressure is as depicted on next **Figure 6**:

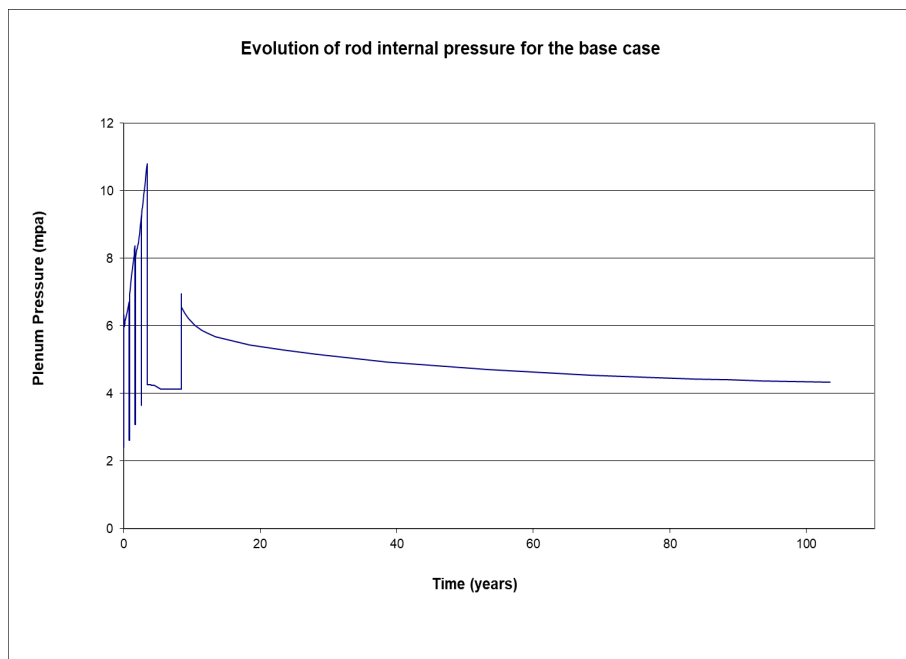


**Fig. 6** Sample result of the benchmark (internal pressure evolution)

The studied fuel rod reaches 107 bar during irradiation, then 40 bar in pool and 70 bar during drying. There is then a drop when entering the colder cask and a progressive decrease following the reduction of the decay heat. The cladding hoop stress follows the same trend, with a peak axial value of 55 MPa during drying and 50 MPa when entering the cask.

For the sensitivity studies, it has been decided to focus on the parameters linked to the hydride reorientation. Based on information in the documents NUREG-2214 and NUREG-2224, it has been decided to choose the axial node with the highest temperature during drying, because it would have the maximum hydride dissolution. Then, its

temperature evolution would be followed until it had decreased by 65°C, the threshold for reprecipitation. At that node and instant, the hoop stress would be extracted, as this is the parameter that would control the appearance of radial hydrides. Indeed, it is accepted that hydrides form in the radial direction if the hoop stress is above a threshold of around 90 MPa when the hydrogen precipitate. This is described in the NUREG documents and the basis for the 90 MPa rule in ISG-11 rev.3. The sensitivity studies were then performed by comparing the values of this result. The results are depicted from Table 2 to Table 4 below.

Table 2: Sensitivities on the environmental conditions

	Parameter	Delta	Hoop Stress at precipitation [MPa]	Time before precipitation [Days after drying]
Case 1	Reference		47.47	293.35
Case 2	Harsher irradiation	Higher Irradiation Power	57.84	500.52
Case 3	Higher residual heat	Rod residual heat +10%	47.54	653.40
Case 4	High cask power	Total cask power +20%	47.57	750.00
Case 5	Strong cask heat transfer	Heat transfer cavity-outside +20%	47.54	1.45
Case 6	Moderate cask convection	Adapted rod axial thermal profile	52.75	94.45

Table 3: Sensitivities on the model effects

	Parameter	Hoop Stress at precipitation [MPa]
Case 1	Nominal	47.83
Case 2	High corrosion	49.08
Case 3	High FGR	53.76
Case 4	High swelling	48.32
Case 5	Low swelling	47.70
Case 6	Low growth	49.02
Case 7	High creep	47.70
Case 8	Low creep	48.61

Table 4: Sensitivities on the fabrication parameters

	Parameter	Delta	Hoop Stress at precipitation [MPa]
Case 1	Nominal		47.83
Case 2b	Clad Out D	-0.03 mm	50.65
	=> Clad thick.	-0.03 mm	
Case 2c	Clad In D	+0.03 mm	54.33
	=> Clad thick.	-0.03 mm	
	=> Gap thick.	+0.03 mm	
Case 3	Fill pressure	+1 bar	49.45
Case 4	Pellet D	+0.015mm	44.20
	=> Gap thick.	-0.015mm	
Case 4b	Pellet D	-0.015mm	50.97
	=> Gap thick.	+0.015mm	
Case 5	Fuel density	-1%	48.87
Case 6	Plenum length	-15 mm	49.07

In terms of developments, Tractebel was able to improve the modelling of corrosion and put in place a method for assessing the risk of hydride reorientation. It also confirmed the validity of its results by comparison with ALCYONE.

The sensitivity studies permitted to estimate the variations of the parameters, but also to determine what are the important parameters. For the fuel rod conditions, see Table 2, those are the irradiation power history and the cask axial temperature profile. Meanwhile, the parameters that only affect the temperature evolution inside the cask will have barely no impact, because the hydride precipitation will still happen at the same temperature and with the same stress. The most important models are those related to fission gas release and corrosion, see Table 3. The most important fabrication parameters are the gap and cladding thicknesses, see Table 4.

The results showed that there is reassurance on the behaviour of representative spent fuel, due to the absence of outward creep during cask storage and the values of hoop stresses well below the threshold of 90 MPa.

### **Spent fuel assemblies FGR evaluation**

The second project is coming from a request of ONDRAF, the entity responsible for waste management in Belgium. It is important for them to have realistic values of FGR because it is correlated with instant release fraction. The latter is an important parameter for the safety evaluation of geological storage.

To achieve this, Tractebel put in place an FGR evaluation system that insert fuel rod irradiation data from the PANTHER core neutronic code into FRAPCON input files. Scripts are used to make the calculations for all fuel rods in an assembly, but also to treat several assemblies in a rod. It is depicted on the next Figure 7. This system can realistically treat dozens of assemblies together, provided that they are of the same design. Indeed, the code input on fuel rod properties has to be created manually.

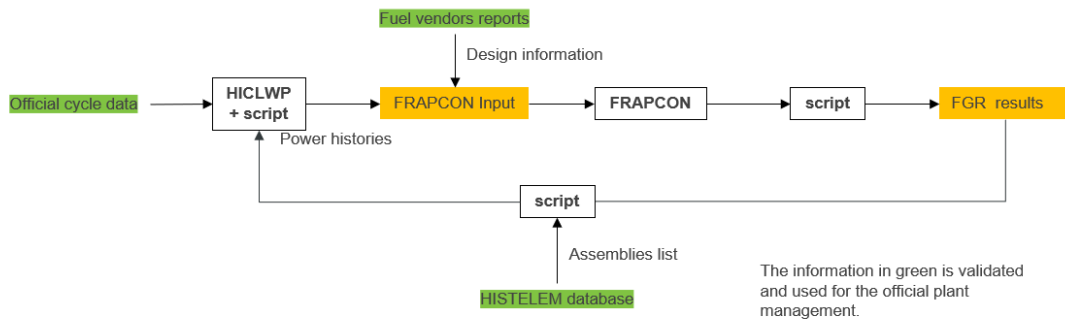


**Fig. 7** Flowchart of the fission gas release evaluation system

This permits to have tabulated results corresponding to all the fuel rods of the assemblies. It can be displayed as in next.

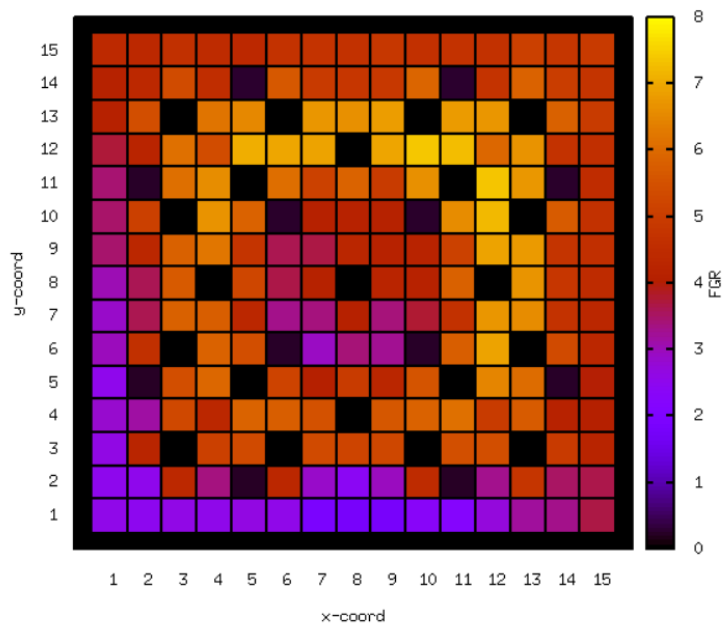


**Fig. 8** Example of FGR results for one assembly

A first validation effort was based on the simulation of fuel rods for which the FGR was measured in Belgium. It led to a calibration of FRAPCON through a bias on the FGR model.

A second validation effort was a comparison with fuel vendor codes. The FGR tool was used to simulate several fuel assemblies while using either FRAPCON or one of the fuel vendor's fuel rod codes. It permitted to make comparisons on the thermal-mechanical part of the simulations. This exercise has shown that the differences were weak in absolute values. The results were similar for the plant corresponding to the previous exercise, but a bit overconservative for the others.

A third work consisted in examining the trends of the results for particular fuel rods, to confirm that they were consistent with the physics.

Currently, there are on-going developments related to MOX and gadolinium fuel assemblies. The evaluation system is already considered able to provide support for spent fuel characterization projects.

## 2.17 Investigating the Applicability of the Master Curve Concept for Ductile Cast Iron – Early Results for 2 Different Test Temperatures,

*Marcel Holzwarth<sup>1</sup>, Uwe Mayer<sup>1</sup>, Wolfram Baer<sup>2</sup>, Stefan Weihe<sup>1</sup>*

*<sup>1</sup>Materials Testing Institute University of Stuttgart (MPA), Germany*

*<sup>2</sup>Federal Institute for Materials Research and Testing (BAM), Germany*

### **Introduction**

Based on the state-of-the-art research and regulations, the application of the fracture mechanics master curve (MC) concept to ferritic ductile cast iron (DCI) is being investigated in a joint research project between MPA Stuttgart and BAM Berlin. This paper outlines the research approach, the planned investigations and first results of the experimental program.

According to the IAEA (2012), the safety assessment of DCI containers for transport as well as interim and final storage of radioactive materials is based on the fracture mechanics criterion of general crack initiation exclusion. In addition, for DCI, the ASME-Code (2019) explicitly requires a safety proof for dynamic loading. Within this context, the focus of the current research project is on the further development of brittle fracture safety assessment methods. The MC concept is currently used as a supplement to the established deterministic ASME reference curve concept and allows an effective statistical consideration of the scatter of the material toughness in the transition regime. Furthermore, it can be used for increased loading velocities as they occur in accidents or crash scenarios, and it is currently the only established standardized method to consider brittle fracture in the ductile-to-brittle transition regime. However, for DCI, a systematic review of potential modifications to the assumptions and the procedure according to ASTM (2023) and an associated validation are still lacking. Therefore, a methodology shall be established to determine and assess dynamic fracture toughness values of DCI in the ductile-to-brittle transition regime using samples extracted from a component.

### **Test Material Specification and Characterization**

The experimental program uses a DCI material of grade GJS-400 (formerly known as GGG-40), which is generally used for transport and storage containers of radioactive materials. 12 casting blocks with a dimension of 820x1550x300 mm were manufactured just for use in this project. To avoid batch influences this was done in a single cast. The tailored manufacturing specification for these casting blocks aimed to produce a homogeneous DCI material close to the material used for nuclear transport and storage

containers. Fig. 1 shows a schematic of the casting blocks. For easier handling 2 smaller blocks (①+②) were extracted from the main block which will be the base for the SE(B)140 specimens and the extraction of smaller specimens.

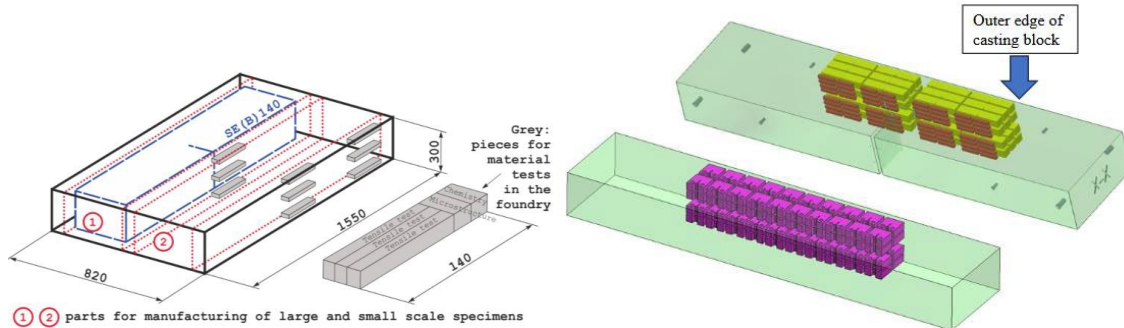


**Fig. 1** Left: Schematic of the GJS400 casting blocks; Right: 2 examples of extraction plans for C(T)25 and SE(B)

After analyzing the homogeneity of the material, it was decided to only use the outer edges of the blocks for specimen extraction, since the biggest gradients were found to be towards the middle. Furthermore, a small gradient along the outer edge has been identified, therefore not the whole outer edge will be used for specimen extraction. The specimen notch will be oriented towards the middle while the ligament will face the outer edges. Due to small gradients also being present from top to bottom side of the block, it was decided to perform extraction

of small specimens in 2 layers, this allows for a comparison of 2 slightly different material states later. Large-scale specimens like SE(B)140 are also part of the experimental program and allow for an assessment of an integral material response. After testing the SE(B)140 specimen, the remaining specimen halves will also be used to manufacture more small-scale specimens. An example for 2 extraction plans is also shown in Fig 1.

### Experimental Program

To start off the experimental program a basic mechanical-technological material characterization will be performed consisting of tensile, Charpy and Pellini tests. The tensile tests will be performed at different temperatures (room temperature, -20 °C, -40°C, and -60 °C), and different strain rates ( $2 \times 10^{-2} \text{ s}^{-1}$ ,  $100 \text{ s}^{-1}$ , and  $10^2 \text{ s}^{-1}$ ). The recorded mechanical characteristics and flow curves will help later to configure the numerical model and the fracture mechanics tests.

To determine the relevant loading rate for brittle fracture, instrumented C(T)25-fracture tests will be performed at different loading rates at a temperature of  $-40^{\circ}\text{C}$ . The loading rates are  $5 \times 10^3 \text{ MPa}\sqrt{\text{ms}}^{-1}$ ,  $5 \times 10^4 \text{ MPa}\sqrt{\text{ms}}^{-1}$  and  $5 \times 10^5 \text{ MPa}\sqrt{\text{ms}}^{-1}$ . To later transfer the relevant loading rate to other specimen sizes or shapes, the time-dependent course of the Weibull stress is assessed via numerical analyses. With this information a series of dynamic fracture tests at  $-40^{\circ}\text{C}$  and additional test temperatures is performed, covering DC(T)9, C(T)25 and C(T)50 specimens at MPA. BAM will perform corresponding SE(B)10 (pre-cracked Charpy), SE(B)25 and SE(B)140 test series to cover the influence of specimen geometry. In total about 400 tests are planned during this project.

To investigate the applicability of the statistical principles of the master curve concept to DCI materials, both the distribution of instability values at a temperature and the variation of median values versus temperature are investigated and checked for compatibility with the evaluation according to ASTM (2023). Subsequently, there will be investigations whether the size effect implemented in ASTM (2023) is applicable or if modifications are needed. The empirical database developed for DCI materials under dynamic loading will also be used to verify the analytical description of the temperature dependence of the fracture toughness. Fractographic investigations will also clarify to what extent the weakest link model, on which the master curve concept is based, can be transferred to DCI materials. Within this framework the transferability of the dynamic master curve equation empirically derived from test data of ferritic steels according to ASTM (2023) to DCI materials is to be assessed and if necessary, material-specific modifications will be proposed.

## Results

On the side of MPA precracking of the specimens was done in accordance with ASTM (2023). Displacement was measured via a highspeed camera recording at 100,000 FPS and force was determined via a load cell and additionally via strain gauges on the specimens. Further strain gauges were placed near the crack tip to gather data on the crack initiation.

KJc,d values and first master curve evaluations were also performed according to ASTM (2023). Fig. 2 shows some of the investigations performed so far, namely the KJc,d values per loading rate and temperature for C(T)25 specimens. Furthermore Fig. 2 shows the standard Master Curve evaluation according to ASTM E1921 performed for the tests at  $-40^{\circ}\text{C}$  via single temperature evaluation and a first attempt at modifying the Master Curve by changing the coefficient of 0.019 to 0.045. So far there is not enough statistical

data to support this modification and changing the coefficient should only be considered one of the ideas which need further investigation. Currently there are also tests being performed at  $-30^{\circ}\text{C}$  to further evaluate the course of the Master Curve for ductile cast iron.

On the BAM Berlin side SE(B)140 testing has been completed. 8 tests were carried out at a temperature of  $-40^{\circ}\text{C}$  and 6 tests at a temperature of  $-60^{\circ}\text{C}$  with a loading rate of approximately  $6.5 \times 10^4 \text{ MPa}\sqrt{\text{m}}\text{s}^{-1}$ . The resulting Force-COD-curves and the corresponding preliminary  $K_{Jc,d}$  values are shown in Fig. 3. An initial qualitative assessment of the values determined so far shows that the scatter of the sample at  $-60^{\circ}\text{C}$  is smaller than at  $-40^{\circ}\text{C}$  and the mean value at  $-60^{\circ}\text{C}$  is lower than at  $-40^{\circ}\text{C}$ .

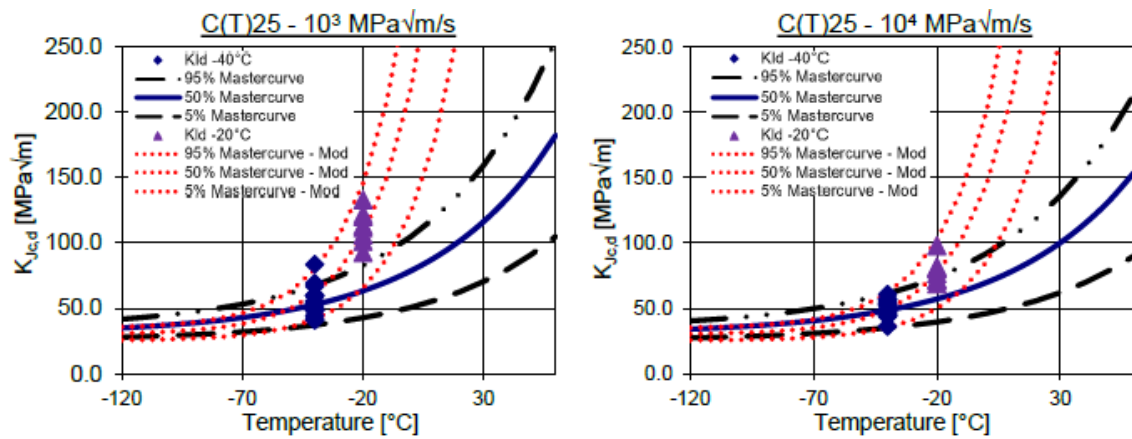


**Fig. 2** Master Curve evaluation for C(T)25 specimens at 2 different loading rates and a test temperature of  $-20^{\circ}\text{C}$  and  $-40^{\circ}\text{C}$  according to ASTM E1921 and a first outlook on how a modified Master Curve could look

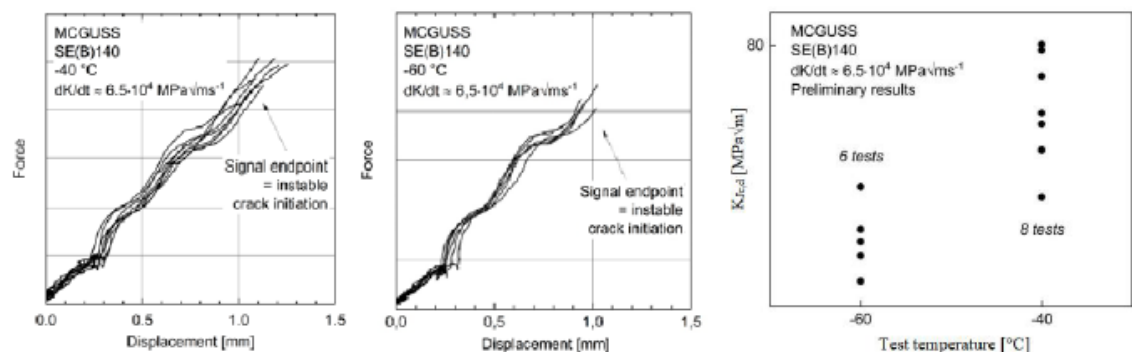


**Fig. 3** Force-COD- curves of the SE(B)140 tests at  $-40^{\circ}\text{C}$  (left) and  $-60^{\circ}\text{C}$  (middle); Preliminary  $K_{Jc,d}$  values of the SE(B)140 tests (right)

## Summary

The overall objective of this joint project is to investigate, further develop and provide a method for brittle fracture safety assessment for DCI materials at increased loading rates. To this end, using the acquired results of the test methods presented above, the applicability of basic approaches of the master curve concept according to ASTM (2023) will be investigated for DCI materials, and, if necessary, modified. The development of such a method aims to make an effective and efficient evaluation available, in which a reference temperature  $T_0$  for material-specific temperature adjustment of the master curve can be determined using a comparatively small number of small fracture mechanics samples. This should make it possible to determine dynamic fracture toughness values of DCI materials in the toughness transition range in a targeted manner using samples extracted from a component.

Once the currently ongoing C(T)25 test series are completed, testing of other geometries (C(T)50, DC(T)9 and Pellini), as well as testing of SE(B)10 and SE(B)25 specimens will begin. These additional results will then further strengthen the statistical database required to validate and modify the master curve concept for DCI.

## Acknowledgements

The joint research project MCGUSS "Investigation of the Master Curve Concept for Ferritic Ductile Cast Iron" with the subprojects "Investigations using C(T) and DC(T) specimens", Project No. 1501650, and "Investigations using SE(B) specimens", Project No. 1501651, was funded by the German Federal Ministry for Environment, Nature Conservation, Nuclear Safety and Consumer Protection (BMUV)) on basis of a decision by the German Bundestag.

## References

- [1] ASME-Code (2019) "ASME Boiler & Pressure Vessel Code III, Division 3 Containments for Transportation and Storage of Spent Nuclear Fuel and High Level Radioactive Material and Waste, WC-2300 Fracture Toughness Requirements for Material".
- [2] ASTM International (2023), "Standard Test Method for Determination of Reference Temperature,  $T_0$ , for Ferritic Steels in the Transition Range", ASTM E1921-23, West Conshohocken, PA: ASTM International, appr. June 1.
- [3] IAEA (2012), "Guidelines for the Safe Design of Shipping Packages against Brittle Fracture," IAEA Specific Safety Guide No. SSG-26, Advisory Material for the IAEA

Regulations for the Safe Transport of Radioactive Material, Vienna, International Atomic Energy Agency, 371-389

## **2.18 An update on metal seal tests performed at BAM and implications for interim storage,**

*Matthias Jaunich, Ilja Sagradov, Milan Goral, Dietmar Wolff, Holger Völzke*

*Bundesamt für Materialforschung (BAM), Germany*

The investigation of the long-term performance of sealing systems employed in containers for radioactive waste and spent nuclear fuel is one research focus area for division 3.4 “Safety of Storage Containers” at the Bundesanstalt für Materialforschung und -prüfung. Metallic seals are in use in interim storage casks for used fuel and high active waste. Their change in performance over time is of high importance for maintaining safe enclosure. Therefore, investigations on these systems were started at BAM to get a general understanding of the relevant processes. Our investigations comprise investigations on different parameters which influence the seal performance and the main part is focussed on the time and temperature dependent behaviour.

In this contribution an update on the performed tests and their respective results will be given in respect to the overview presented in 2020.

The understanding of the long-term behaviour of the sealing systems and the performance evaluation during interim storage and subsequent transportation are our goals.

**Gesellschaft für Anlagen-  
und Reaktorsicherheit  
(GRS) gGmbH**

Schwertnergasse 1  
**50667 Köln**

Telefon +49 221 2068-0

Telefax +49 221 2068-888

Boltzmannstraße 14

**85748 Garching b. München**

Telefon +49 89 32004-0

Telefax +49 89 32004-300

Kurfürstendamm 200

**10719 Berlin**

Telefon +49 30 88589-0

Telefax +49 30 88589-111

Theodor-Heuss-Straße 4

**38122 Braunschweig**

Telefon +49 531 8012-0

Telefax +49 531 8012-200

[www.grs.de](http://www.grs.de)